J. Fluid Mech. (2009), *vol.* 638, *pp.* 267–303.
doi:10.1017/S0022112009990838

The pre-transitional Klebanoff modes and other boundary-layer disturbances induced by small-wavelength free-stream vorticity

PIERRE RICCO†

Department of Mechanical Engineering, King's College London, Strand, London WC2R 2LS, UK

(Received 25 November 2008; revised 16 June 2009; accepted 16 June 2009)

The response of the Blasius boundary layer to free-stream vortical disturbances of the convected gust type is studied. The vorticity signature of the boundary layer is computed through the boundary-region equations, which are the rigorous asymptotic limit of the Navier–Stokes equations for low-frequency disturbances. The method of matched asymptotic expansion is employed to obtain the initial and outer boundary conditions. For the case of forcing by a two-dimensional gust, the effect of a wall-normal wavelength comparable with the boundary-layer thickness is taken into account. The gust viscous dissipation and upward displacement due to the mean boundary layer produce significant changes on the fluctuations within the viscous region. The same analysis also proves useful for computing to second-order accuracy the boundary-layer response induced by a three-dimensional gust with spanwise wavelength comparable with the boundary-layer thickness. It also follows that the boundary-layer fluctuations of the streamwise velocity match the corresponding free-stream velocity component. The velocity profiles are compared with experimental data, and good agreement is attained.

The generation of Tollmien–Schlichting waves by the nonlinear mixing between the two-dimensional unsteady vorticity fluctuations and the mean flow distortion induced by localized wall roughness and suction is also investigated. Gusts with small wall-normal wavelengths generate significantly different amplitudes of the instability waves for a selected range of forcing frequencies. This is primarily due to the disparity between the streamwise velocity fluctuations in the free stream and within the boundary layer.

1. Introduction

The laminar–turbulent transition in boundary layers is an extremely complex phenomenon which has attracted the attention of scientists and engineers for over a century. Its understanding and prediction are of relevant academic interest and of utmost importance for the design of efficient thermo-fluid systems. Indeed, the boundary layer is responsible for much of the flow energy transfer and dissipation, crucially affecting the performance of mechanical, aeronautical, civil and chemical engineering systems. It is therefore important to determine whether a flow will be laminar, transitional or turbulent, since the kinematic and thermal flow properties change drastically in each regime.

† Email address for correspondence: pierre.ricco@kcl.ac.uk

The first research efforts were directed towards the initial stage of transition, namely the linear instability of a purely laminar boundary layer, where the small-amplitude disturbances were assumed to be already present within the viscous layer. The Orr–Sommerfeld stability equation for a viscous flow was derived from the Navier–Stokes equations by Orr (1907) and Sommerfeld (1908). Tollmien (1929) and Schlichting (1933) calculated the neutral curve of instability for the Blasius boundary layer, and the unstable waves were thus named Tollmien–Schlichting (TS) waves. Later, Schubauer & Skramstad (1947) were able to excite them in a wind tunnel by introducing sound into the boundary layer through a small hole in the flat plate. In this carefully designed environment, the free-stream turbulence was reduced to a very low level, $\sim$0.01–0.03%.

The most relevant of the recent experimental studies on the controlled generation of instability waves are the one by Wiegel & Wlezien (1993) for acoustic disturbances and the ones by Dietz (1996, 1998, 1999) for vortical disturbances. In the latter, a ribbon was vibrated in the free stream and roughness was placed at the wall to trigger two-dimensional TS waves. Quantitative data of the amplitude of the instability waves were thus obtained for the first time. The TS waves have therefore been generally acknowledged as the key feature in laminar–turbulent transition when the level of the external perturbations is reduced to a minimum.

Experiments under the influence of more intense free-stream turbulence have shown that spanwise-alternating low- and high-speed disturbances within the boundary layer may significantly amplify and distort the flow (Dryden 1936; Taylor 1939). Renewed interest has risen with the studies by Bradshaw (1965), Klebanoff (1971), Arnal & Juillen (1978), Kendall (1985, 1990, 1991), Gulyaev *et al.* (1989) and Westin *et al.* (1994), which confirmed that these structures are of low frequency and are streamwise elongated, as the streamwise velocity component is much larger than the wall-normal and spanwise velocity components. The terms laminar streaks, breathing modes and Klebanoff modes have been adopted. It is believed that small-amplitude Klebanoff modes initially evolve linearly, and when their amplitude exceeds a threshold amplitude, they may interact nonlinearly and be precursors of an alternative route to turbulence, often called bypass transition. More recent experimental investigations have been conducted by Watmuff (1998), Matsubara & Alfredsson (2001), Inasawa *et al.* (2003), Fransson, Matsubara & Alfredsson (2005), Mans *et al.* (2005), Anthony, Jones & LaGraff (2005), Volino (2005), Hernon, Walsh & McEligot (2007) and Huang & Johnson (2007). Numerical simulations of the Klebanoff modes have also appeared (see Jacobs & Durbin 2001, Nagarajan, Lele & Ferziger 2007 and Ovchinnikov, Choudhari & Piomelli 2008 for direct numerical simulations and Lardeau, Li & Leschziner 2007 for large-eddy simulations), where the inflow condition which models the initial stage of the streak evolution was provided by a superposition of Orr-Sommefeld and Squire modes. Fasel (2002) and recently Liu, Zaki & Durbin (2008) used direct numerical simulations to study the breakdown to turbulence produced by the interaction of TS waves with Klebanoff modes.

The mathematical modelling of the Klebanoff modes has provoked much interest within the fluid mechanics community. Some formulations take into account the free-stream disturbances, which generate the Klebanoff modes inside the boundary layer. The relevant boundary value problem is inhomogeneous with respect to the outer boundary conditions, which synthesize the interaction between the boundary layer and the free-stream flow. The theoretical work by Crow (1966), prompted by the experiments by Bradshaw (1965), was probably the first effort directed at the entrainment of free-stream disturbances in the boundary layer. The focus was

on small-amplitude, steady free-stream disturbances penetrating into the Blasius boundary layer. The streamwise velocity was found to grow linearly with the downstream distance. Goldstein, Leib & Cowley (1992) showed that Crow's linear solution is valid only within a short distance from the leading edge (see also Goldstein & Leib 1993). The formation of laminar streaks was also investigated by Choudhari (1996) using the linearized unsteady boundary-layer (LUBL) equations and by Leib, Wundrow & Goldstein (1999) using the linearized unsteady boundary-region (LUBR) equations. These equations are a rigorous asymptotic limit of the Navier–Stokes equations for low-frequency disturbances. The latter equations account for the effects of spanwise viscous diffusion, namely for spanwise wavelengths comparable with the boundary-layer thickness, while in the boundary-layer equations these effects are negligible because the spanwise wavelength is asymptotically larger than the boundary-layer thickness. Leib *et al.* (1999) obtained the free-stream boundary conditions by asymptotic matching between the boundary-layer displacement and the outer flow. The external vortical flow is not independent of the viscous wall layer because it is continuously influenced by the fluctuations within the boundary layer. Their analysis reveals that the amplification of the streamwise velocity within the boundary layer, recognized as the distinguished feature of the Klebanoff modes, is due to the spanwise velocity component of the free-stream gust. Other works on the generation of vorticity disturbances by free-stream fluctuations are by Goldstein & Wundrow (1998), Wundrow & Goldstein (2001), Wu & Choudhari (2003) and Goldstein & Sescu (2008). Similar structures have recently been studied, such as the thermal Klebanoff modes (Ricco & Wu 2007; Ricco, Tran & Ye 2009), which may be generated by free-stream gusts interacting with a compressible laminar boundary layer.

The spatial development of the streaks has also been studied by the optimal growth theory (Andersson, Berggren & Henningson 1999; Luchini 2000). These perturbations are allowed to vanish in the free stream and are generated by an iterative procedure to obtain the maximum growth at a specified downstream distance. The streamwise velocity profile agrees well with the low-frequency experimental data in the core of the boundary layer, even though the penetration of the free-stream vortical disturbances is not included in the model.

Another related interesting issue is the scattering of TS waves. Since low-frequency boundary-layer vorticity fluctuations (such as the Klebanoff modes) are generated by free-stream vortical gusts propagating at the free-stream mean velocity, their wavelength is much larger than the wavelength of the TS waves. Therefore, for free-stream-induced vorticity disturbances to trigger TS waves, a wavelength conversion mechanism is necessary to introduce the correct length scale into the problem. Such a mechanism is called receptivity. Its objectives are (i) to explain the process of excitation of the instability waves and (ii) to predict the TS-wave amplitude. The frequency of the instability waves is provided by the unsteady free-stream disturbance, while the wavelength is usually extracted from a steady perturbation, often located at the wall (Goldstein 1985), or by a leading-edge adjustment mechanism induced by the non-parallel effects of the mean flow (Goldstein 1983; Ricco & Wu 2007). The induced wave has therefore the frequency and wavelength of the TS wave, so that it grows exponentially as predicted by linear stability theory.

The pioneering works on receptivity have dealt with unsteady forcing of the acoustic type (Goldstein 1983, 1985; Ruban 1985). Only recently has the interest been directed to the TS-wave generation by free-stream vorticity. This represents a more involved problem, in that the boundary-layer response to a sound wave

can be often approximated by a Stokes layer, while the signature of the Klebanoff modes is more difficult to compute. Kerschen (1991) presented the first asymptotic receptivity study involving a gust, which was studied in more detail by Duck, Ruban & Zhikharev (1996) using the triple-deck formulation. Choudhari (1996), following his acoustic receptivity work (Choudhari & Streett 1992), investigated the receptivity to three-dimensional gusts interacting with wall inhomogeneities by the finite-Reynolds-number (FRN) approach. Extensive theoretical work has been carried out by Wu (2001*a*,*b*) for gusts interacting with localized and distributed wall roughness. Second-order triple-deck calculations were employed for the first time to obtain very accurate quantitative comparisons between the theoretical results and the experimental data by Dietz (1999).

The wall-normal wavelength λ_y^* of the gust was not given in Dietz (1999), but from the profile of the free-stream disturbance it could be inferred that λ_y^* was about 10 times the boundary-layer thickness. It is therefore likely that the wavelength was large enough for the effects of boundary-layer displacement and viscous dissipation on the free-stream gust to be neglected. The excellent agreement between Dietz's data and the theoretical results by Wu (2001*a*,*b*, where these effects were not taken into account) confirms this hypothesis. The wavelength λ_y^* being large translates into an asymptotically small scaled parameter $\kappa_2 = \sqrt{2\pi\nu\lambda_x^*/U_\infty}/\lambda_y^* \approx \delta^*/\lambda_y^*$ (Leib *et al.* 1999). (Here ν is the kinematic viscosity of the fluid, λ_x^* is the streamwise wavelength, U_∞ is the mean free-stream velocity and $\delta^* = \sqrt{x^*\nu/U_\infty}$ is a measure of the boundary-layer thickness.) In this limit, the boundary-layer equations may be used instead of the boundary-region equations; namely pressure fluctuations do not play a role at leading order.

In the present work, we focus on four objectives related to the response of the boundary layer to free-stream vortical gusts. They can be schematically listed as follows:

(*a*) We first investigate the boundary-layer response to a two-dimensional convected gust with a wall-normal wavelength comparable with the boundary-layer thickness, $\lambda_y^* = O(\delta^*)$ ($\kappa_2 = O(1)$). The analysis accounts for the effects of free-stream viscous dissipation and of upward displacement of the gust due to the underlying boundary layer.

(*b*) The three-dimensional form of the disturbances described above proves useful to obtain a better representation of the vorticity fluctuations produced by a three-dimensional gust with small wall-normal and spanwise wavelengths ($\kappa_2, \kappa = O(1)$, where for κ the spanwise wavelength λ_z^* substitutes λ_y^* in the definition of κ_2). More precisely, as the asymptotic expansion is carried out with respect to the small frequency, these components synthesize the second-order effects. It follows that the mathematical framework can now account for disturbances of higher frequencies than in previous studies. The first-order terms are found to be $O(\lambda_x^*/\lambda_z^*)$ (with $\lambda_x^* \gg \lambda_z^*$) larger than the free-stream disturbances, while the second-order terms are of the same order of the outer gust fluctuations. The inclusion of these terms is also important because, in the three-dimensional case, the streamwise velocity of the Klebanoff mode matches the corresponding component of the free-stream gust. This matching is not possible if only the leading-order component is employed because the latter vanishes in the free stream. This gives a more realistic representation of the streak profile because these terms are dominant near the free stream. Arguably, Leib *et al.* (1999) focused their analysis only on part of the vorticity signature because they sought to reproduce experimental data of the peak of the laminar streaks located in the middle of the boundary layer.

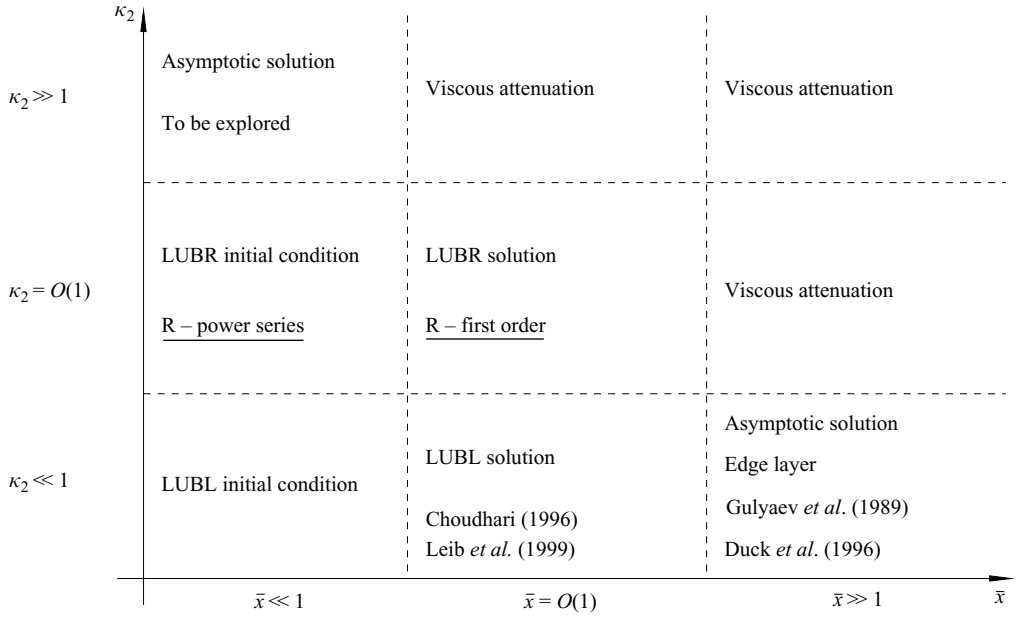

FIGURE 1. Schematic of the asymptotic regions for different κ_2 and $\bar{x}$ for boundary-layer response to a two-dimensional gust. Here and in the following figure, the parts indicated with R and underlined denote the results of the present analysis.

We are further interested in the physical mechanism responsible for the formation of the outer fluctuations, which will be revealed to be subtler than for the first-order quantities. It will be shown that pressure fluctuations play a key role, while they are irrelevant for the generation of the first-order components. The present analysis also works towards the objective of explaining the mechanism of bypass transition. Indeed, as for example pointed out by Jacobs & Durbin (2001), while the low-frequency disturbances distort the flow, the high-frequency ones may be responsible for triggering the secondary instability when the streaks move towards the outer portion of the boundary layer. It is therefore of great interest to compute accurately the vorticity signature of the high-frequency component, a task which is tackled by solving for the second-order components.

Figures 1 and 2 show schematics of the asymptotic regions for the response of a two-dimensional and a three-dimensional free-stream gust, respectively. The regions are defined according to the values of κ, κ_2 and $\bar{x} = 2\pi x^*/\lambda_x^* = O(1)$, the scaled streamwise distance from the leading edge. In the figures, the underlined parts indicate the results of the present analysis and the notations LUBL and LUBR refer to the LUBL and LUBR equations. At $\bar{x} \ll 1$, the initial conditions must be imposed to solve the equations numerically, and the solution attains an asymptotic self-similarity solution in the limit $\kappa \gg 1$, $\kappa^2\bar{x} = O(1)$ (see §4.1.2 and Leib *et al.* 1999, p. 184). At $\bar{x} = O(1)$, the LUBR solution is valid for $\kappa, \kappa_2 = O(1)$ and the LUBL solution is valid for $\kappa, \kappa_2 \ll 1$, while for $\bar{x} \gg 1$ the disturbances for $\kappa, \kappa_2 \ll 1$ attain an asymptotic solution (edge-layer confinement) and decay by viscous effects when $\kappa, \kappa_2 = O(1)$.

(*c*) Another task is to compare the streamwise velocity profiles of the Klebanoff modes with experimental data. Of particular interest is the unique experimental dataset by Westin *et al.* (1994, figure 12*a*, p. 210) of the fluctuating energy at a single frequency of free-stream forcing.

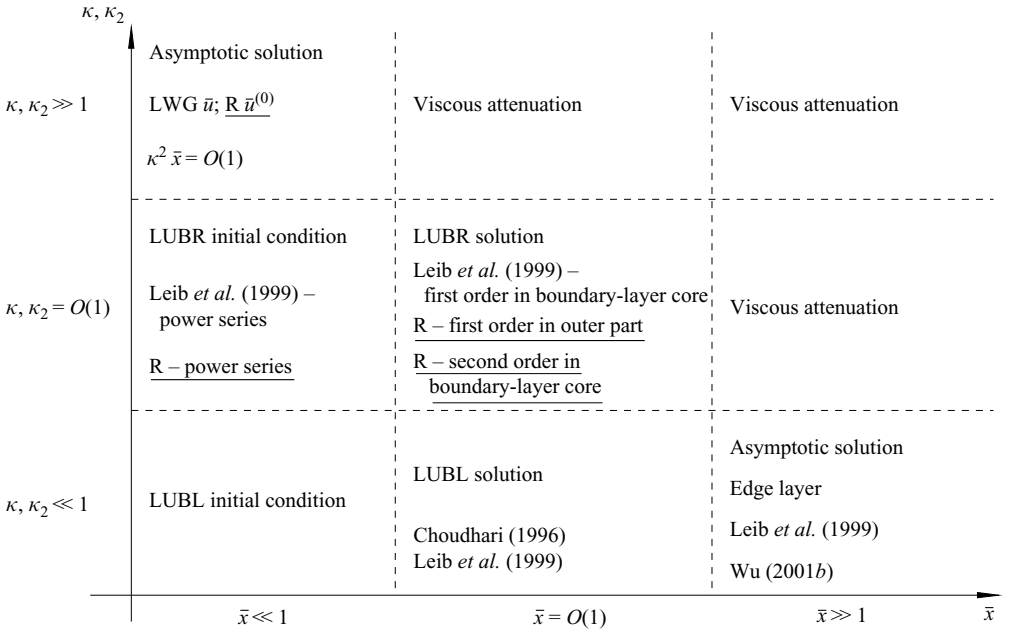

FIGURE 2. Schematic of the asymptotic regions for different κ, κ_2 and $\bar{x}$ for three-dimensional Klebanoff modes.

(*d*) The influence of wall-normal wavelengths comparable with the boundary-layer thickness is investigated on the amplitude of TS waves scattered by the nonlinear interactions between the two-dimensional vorticity fluctuations and the mean flow distortion produced by localized wall perturbations. As outlined above, the wall-normal wavelength was much larger than the boundary-layer thickness in previous receptivity studies.

We compute the boundary-layer velocity signature by the LUBR equations with proper outer boundary conditions to account for the unsteady free-stream forcing. We consider two kinds of localized wall inhomogeneities, wall roughness and wall suction, and employ the FRN approach developed by Choudhari & Streett (1992) to compute the amplitude of the scattered TS waves. Different from triple-deck theory, where the Reynolds number is treated as an asymptotically large quantity (and is therefore scaled out of the problem), in the FRN approach the Reynolds number appears in the equations as a parameter. Although the FRN framework is not as mathematically rigorous as the triple-deck theory because of its *ad hoc* approach to some aspects of the receptivity problem (such as the exclusion of the non-parallel terms), results from the two methods show satisfactory quantitative agreement at first order (Wu 2001*a*). The triple-deck approach is perfectly suited for those cases in which the vorticity response is given by analytic formulas (Duck *et al.* 1996; Wu 2001*a*,*b*). However, the FRN formulation is arguably simpler to implement when the vorticity response is given by a numerical solution, like in the present case.

The paper is structured as follows. The mathematical formulation is presented in section § 2: the framework of the LUBR equations with appropriate outer and initial conditions is outlined in § 2.1, while the FRN receptivity approach is described in § 2.2. The numerical procedures for solving the LUBR equations are found in § 3.1. A brief description of the methodology for solving the homogeneous and inhomogeneous

Orr–Sommerfeld equations, for the stability and receptivity calculations respectively, is given in § 3.2. In § 4.1, the boundary-layer vorticity signatures induced by a two-dimensional gust (§ 4.1.1) and a three-dimensional gust (§ 4.1.2) are discussed, and the comparison with the available experimental data is presented in § 4.1.3. Section § 4.2 discusses the receptivity results, i.e. the effects of the free-stream gust properties on the amplitude of the TS waves. A summary is given in § 5.

2. Mathematical formulation

2.1. *Boundary-layer response to free-stream convected gusts*

As in Leib *et al.* (1999), the mathematical framework for the response of a laminar boundary layer to small free-stream vortical gusts is the LUBR equations. The formulation follows closely the one by Leib *et al.* (1999), and it is extended to find the outer boundary conditions ((2.13) and (2.21)–(2.23)) and the initial conditions ((2.30) and Appendix B) for the components denoted as $\{\overline{u}^{(0)}, \overline{v}^{(0)}, \overline{w}^{(0)}, \overline{p}^{(0)}\}$, which are of second order in the core of the boundary layer and of first order in the outer portion of it.

A flow of uniform velocity U_∞ past an infinitely thin flat plate is considered. Superimposed on U_∞ are homogeneous, statistically stationary vortical fluctuations. These perturbations are of the gust type; i.e. they are convected by the mean flow. The flow is assumed to be incompressible and is described in terms of a Cartesian coordinate system, i.e. by a position vector $\boldsymbol{x} = x\hat{\boldsymbol{i}} + y\hat{\boldsymbol{j}} + z\hat{\boldsymbol{k}} = x_1\hat{\boldsymbol{i}} + x_2\hat{\boldsymbol{j}} + x_3\hat{\boldsymbol{k}}$, where x, y and z (or x_1, x_2 and x_3) define the streamwise, wall-normal and spanwise directions. Lengths are scaled by λ_z^*, the spanwise wavelength of gust, so that the scaled spanwise wavenumber is $k_3 = 2\pi$. The velocities are scaled by U_∞, and the pressure is normalized by $\rho^* U_\infty^2$, where ρ^* is the free-stream density, and the time by λ_z^*/U_∞. The symbol * indicates a dimensional quantity.

Mathematically, the vorticity fluctuations can be represented as a superposition of sinusoidal disturbances:

$$\boldsymbol{u} - \hat{\boldsymbol{i}} = \epsilon_g \boldsymbol{u}_\infty(x - t, y, z) = \epsilon_g \hat{\boldsymbol{u}}^\infty \mathrm{e}^{\mathrm{i}(\boldsymbol{k}\cdot\boldsymbol{x} - k_1 t)} + \text{c.c.},$$

where $\epsilon_g \ll 1$ indicates the amplitude of the gust and c.c. denotes the complex conjugate. The problem is formulated for a single Fourier component of the free-stream turbulence. The gust vector $\hat{\boldsymbol{u}}^\infty = \{\hat{u}_1^\infty, \hat{u}_2^\infty, \hat{u}_3^\infty\}$ can be expressed as

$$\hat{\boldsymbol{u}}^\infty = \{\sin\theta_g \cos\phi_g, \cos\theta_g, \sin\theta_g \sin\phi_g\},$$

upon introducing the polar angle $\theta_g (0 < \theta_g < \pi)$ and the azimuthal angle ϕ_g $(-\pi < \phi_g < \pi)$ of orientation (Choudhari 1996). It further occurs that

$$|\hat{\boldsymbol{u}}^\infty| = \sqrt{\left(\hat{u}_1^\infty\right)^2 + \left(\hat{u}_2^\infty\right)^2 + \left(\hat{u}_3^\infty\right)^2} = 1 \tag{2.1}$$

and that the continuity equation can be written as

$$\hat{\boldsymbol{u}}^\infty \cdot \boldsymbol{k} = 0. \tag{2.2}$$

For a two-dimensional gust (i.e. for a gust with no spanwise velocity component, $\hat{u}_3^\infty = 0$, and with an infinitely long spanwise wavelength, $k_3/k_1 \to 0$), $\phi_g = 0$ and θ_g describes $\hat{\boldsymbol{u}}^\infty$.

We focus on low-frequency (i.e. long-wavelength) disturbances with $k_1 \ll 1$, as these are the ones that can penetrate the most into the boundary layer to form the laminar streaks. The Reynolds number is defined as $R_\lambda \equiv U_\infty \lambda_z^*/\nu$. We take R_λ to be

asymptotically large, i.e. $R_\lambda \gg 1$. Following Leib *et al.* (1999), the flow is studied at downstream locations at which the boundary-layer thickness $\delta^* = O(\lambda_z^*)$, i.e. where $x/R_\lambda = O(1)$, which means that the diffusion in the spanwise direction is of the same order as that in the wall-normal direction. A distinguished scaling is $k_1 = O\left(R_\lambda^{-1}\right)$ or, equivalently, $\overline{x} = k_1 x = O(1)$ because the laminar streaks evolve downstream on a length scale which is comparable with the streamwise wavelength of the gust. Due to the disparity between the spanwise and streamwise scales, $O(\epsilon_g)$ fluctuations in the free stream can generate $O(\epsilon_g/k_1)$ streamwise velocity disturbances within the boundary layer. We assume that the amplitude of disturbances is much smaller than the amplitude of the mean flow, so that the equations can be linearized. The condition for linearization, $\epsilon_g/k_1 \ll 1$, becomes $\epsilon_g R_\lambda \ll 1$.

The unsteady perturbations interact with the flat plate. The flow field can be described by the rapid distortion theory of turbulence. When the theory is applied to a flow over an infinitely thin flat plate, the velocity at leading order is expressed as (Goldstein 1978)

$$\boldsymbol{u} = \hat{\boldsymbol{i}} + \epsilon_g(\boldsymbol{u}_\infty + \nabla\phi).$$

The potential function ϕ arises from the interaction of the gust with the flat plate and must be included in order to satisfy the no-penetration boundary condition at the plate. As shown by Leib *et al.* (1999), for $x \gg 1$

$$\phi = \frac{\hat{u}_2^\infty \mathrm{e}^{-\Gamma y}}{\Gamma} \mathrm{e}^{\mathrm{i}k_1(x-t)+\mathrm{i}k_3 z} \; + \; \text{c.c.}, \quad \Gamma \equiv \left(k_1^2 + k_3^2\right)^{1/2}.$$

The streamwise and spanwise slip velocities at the surface of the plate ($y = 0$) are given by

$$u_1^{(1)}(0) = \hat{u}_1^\infty + \frac{\mathrm{i}k_1}{\Gamma}\hat{u}_2^\infty, \quad u_3^{(1)}(0) = \hat{u}_3^\infty + \frac{\mathrm{i}k_3}{\Gamma}\hat{u}_2^\infty. \tag{2.3}$$

These velocities are reduced to zero across the boundary layer. A similarity solution exists for this flow with the similarity variable defined as

$$\eta \equiv y\left(\frac{R_\lambda}{2x}\right)^{1/2} = y^*\sqrt{\frac{U_\infty}{2\nu x^*}}. \tag{2.4}$$

The mean flow solution is expressed as

$$U = F'(\eta), \quad V = (2xR_\lambda)^{-1/2}\left(\eta F' - F\right), \tag{2.5}$$

where the prime indicates differentiation with respect to η and U and V represent the mean streamwise and wall-normal velocity components. It follows from the x-momentum equation that F is governed by

$$F''' + FF'' = 0. \tag{2.6}$$

The boundary conditions are

$$F(0) = F'(0) = 0, \text{ and } F' \to 1 \text{ as } \eta \to \infty.$$

For a single Fourier component of the disturbance, the solution in the boundary layer is expressed as

$$\begin{aligned}\{u, v, w, p\} &= \{U, V, 0, -1/2\} \\ &+ \epsilon_g \left\{ \overline{u}_0(\overline{x}, \eta), \left(\frac{2\overline{x}k_1}{R_\lambda}\right)^{1/2} \overline{v}_0(\overline{x}, \eta), \overline{w}_0(\overline{x}, \eta), \overline{p}_0(\overline{x}, \eta) \right\} \mathrm{e}^{\mathrm{i}(k_3 z - k_1 t)} \; + \; \text{c.c.} + \ldots .\end{aligned} \tag{2.7}$$

Boundary-layer disturbances with $\lambda_z^* \gg \delta^*$ at $\bar{x} = O(1)$ are described by the LUBL equations (see (4.5) and (4.6) in Leib *et al.* 1999, p. 176). When $\delta^* = O(\lambda_z^*)$, the LUBR equations must be employed. These equations (Kemp 1951) represent the asymptotically rigorous limit of the Navier–Stokes equations for disturbances with streamwise wavelength which is long compared with both the boundary-layer thickness and the spanwise wavelength. The LUBR equations are well suited for studying the Klebanoff modes, since experimental evidence (Kendall 1985; Westin *et al.* 1994) suggests that when the streaky structures are well developed within the boundary layer, they are of low frequency and their spanwise wavelength is $O(\delta^*)$. The velocity and pressure disturbances are expressed as (Gulyaev *et al.* 1989)

$$\left.\begin{aligned} \{\bar{u}_0, \bar{v}_0\} &= C^{(0)}\left\{\bar{u}^{(0)}, \bar{v}^{(0)}\right\} + (\mathrm{i}k_3/k_1)C\{\bar{u}, \bar{v}\}, \\ \bar{w}_0 &= -(ik_1/k_3)C^{(0)}\bar{w}^{(0)} + C\bar{w}, \\ \bar{p}_0 &= (k_1/R_\lambda)C^{(0)}\bar{p}^{(0)} + \mathrm{i}\kappa\,(k_1/R_\lambda)^{1/2}\,C\bar{p}, \end{aligned}\right\} \tag{2.8}$$

where $\kappa \equiv k_3/(k_1 R_\lambda)^{1/2} = \sqrt{2\pi\nu\lambda_x^*/U_\infty}/\lambda_z^* = O(1)$, $C^{(0)} = \hat{u}_1^\infty + \mathrm{i}k_1\hat{u}_2^\infty/\Gamma$ and $C = \hat{u}_3^\infty + \mathrm{i}k_3\hat{u}_2^\infty/\Gamma$. The terms proportional to the components $\{\bar{u}, \bar{v}, \bar{w}, \bar{p}\}$ have been studied by Leib *et al.* (1999) and represent the dominant part of the vorticity and pressure fluctuations in the core of the boundary layer. The terms proportional to the components $\{\bar{u}^{(0)}, \bar{v}^{(0)}, \bar{w}^{(0)}, \bar{p}^{(0)}\}$ indicate the second-order part in the middle of the boundary layer and the leading-order part of the Klebanoff modes at the outer edge of the boundary layer. They are solved for in the following for the first time. Both $\{\bar{u}^{(0)}, \bar{v}^{(0)}, \bar{w}^{(0)}, \bar{p}^{(0)}\}$ and $\{\bar{u}, \bar{v}, \bar{w}, \bar{p}\}$ satisfy the LUBR equations:

$$\frac{\partial\bar{u}}{\partial\bar{x}} - \frac{\eta}{2\bar{x}}\frac{\partial\bar{u}}{\partial\eta} + \frac{\partial\bar{v}}{\partial\eta} + \bar{w} = 0, \tag{2.9}$$

$$\left(-\mathrm{i} + \kappa^2 - \frac{\eta F''}{2\bar{x}}\right)\bar{u} + F'\frac{\partial\bar{u}}{\partial\bar{x}} - \frac{F}{2\bar{x}}\frac{\partial\bar{u}}{\partial\eta} - \frac{1}{2\bar{x}}\frac{\partial^2\bar{u}}{\partial\eta^2} + F''\bar{v} = 0, \tag{2.10}$$

$$\left(-\mathrm{i} + \kappa^2 + \frac{(\eta F')'}{2\bar{x}}\right)\bar{v} + F'\frac{\partial\bar{v}}{\partial\bar{x}} - \frac{F}{2\bar{x}}\frac{\partial\bar{v}}{\partial\eta} - \frac{1}{2\bar{x}}\frac{\partial^2\bar{v}}{\partial\eta^2} - \frac{\eta(\eta F')' - F}{(2\bar{x})^2}\bar{u} + \frac{1}{2\bar{x}}\frac{\partial\bar{p}}{\partial\eta} = 0, \tag{2.11}$$

$$(-\mathrm{i} + \kappa^2)\bar{w} + F'\frac{\partial\bar{w}}{\partial\bar{x}} - \frac{F}{2\bar{x}}\frac{\partial\bar{w}}{\partial\eta} - \frac{1}{2\bar{x}}\frac{\partial^2\bar{w}}{\partial\eta^2} - \kappa^2\bar{p} = 0. \tag{2.12}$$

The LUBR equations simplify to the boundary-layer equations for $\kappa \to 0$ and $\bar{x} = O(1)$, namely in the limit of vanishing spanwise diffusion. For the response to a two-dimensional gust, $\bar{w}^{(0)}, \bar{u}, C, \kappa$ vanish, and $C^{(0)} = \mathrm{i}\exp(-\mathrm{i}\theta_g) = \hat{u}_1^\infty + \mathrm{i}\hat{u}_2^\infty$.

Note that the LUBR equations correctly include the non-parallel terms, which are the expression of the downstream evolution of the boundary layer. These terms play a leading-order role especially in the outer portion of the boundary layer (Wu 2001*a*). Therefore, the Orr–Sommerfeld and Squire equations, where the non-parallel effects are absent, cannot describe the laminar streaks. However, the Orr–Sommerfeld equation can be successfully employed for the receptivity analysis because the TS-wave generation is a local process, whereas the Klebanoff modes dynamics is non-local. The complete evolution from the proximity of the leading edge must be considered because the free-stream disturbances continuously interact with the boundary layer. Numerical evidence of the failure of the parallel approximation to describe the laminar streaks at the beginning of their evolution and of its validity further downstream is given in § 4.2.

The boundary-region system (2.9)–(2.12) requires free-stream boundary and initial conditions, which are studied in § 2.1.1 and § 2.1.2.

2.1.1. *Outer boundary conditions*

To derive the outer boundary conditions for (2.9)–(2.12), the velocity field is expanded as (Leib *et al.* 1999)

$$\boldsymbol{u} = (\partial\Psi/\partial y, -\partial\Psi/\partial x, 0) + \epsilon_g \boldsymbol{u}^{(0)} \mathrm{e}^{\mathrm{i}(k_3 z - k_1 t)} + \text{c.c.} + \ldots,$$

where Ψ is the streamfunction of the mean flow,

$$\Psi = y - \beta \mathrm{Re}\left[2\,(x + \mathrm{i}y)\,/R_\lambda\right]^{1/2},$$

with Re indicating the real part and $\beta = 1.217\ldots$. As $y \to 0$, it reduces to $\Psi \sim y - \beta\,(2x/R_\lambda)^{1/2} = y^{(0)}/(k_1 R_\lambda)^{1/2}$ upon introducing the new scaled variable:

$$y^{(0)} \equiv (2\overline{x})^{1/2}\overline{\eta}, \quad \overline{\eta} \equiv \eta - \beta.$$

It is found (Leib *et al.* 1999, p. 181) that the free-stream velocity components are

$$\boldsymbol{u}^{(0)} = \hat{\boldsymbol{u}}^{\infty} \mathrm{e}^{\mathrm{i}\left(\overline{x} + \kappa_2 y^{(0)}\right) - \left(\kappa^2 + \kappa_2^2\right)\overline{x}} \quad \text{as} \quad k_1 y \to 0.$$

The exponent $-(\kappa^2 + \kappa_2^2)\overline{x}$ accounts for the viscous attenuation, while the boundary-layer displacement effect is absorbed into the exponent $i\kappa_2 y^{(0)}$. If $k_1 \gg R_\lambda^{-1}$, then $\kappa, \kappa_2 \ll 1$ so that both effects can be neglected at leading order for $\overline{x} = O(1)$. At $\overline{x} = O(1)$, $\kappa_2 = O(1)$ translates into $\delta^* = O(\lambda_y^*)$, so that the boundary layer displaces the vortical disturbances upward and the viscous effects are induced by the small λ_y^* of the gust.

The boundary conditions as $\eta \to \infty$ for the LUBR equations are obtained by solving the large-η LUBR equations, which are found by substituting $F \to \overline{\eta}$ into (2.9)–(2.12). The solutions to the large-η equations which match the free-stream solutions are

$$\overline{u}^{(0)} = \frac{\mathrm{e}^{\mathrm{i}\overline{x}}}{\kappa_2 - \mathrm{i}|\kappa|}\left(\kappa_2 \mathrm{e}^{\mathrm{i}\kappa_2 y^{(0)} - \left(\kappa^2 + \kappa_2^2\right)\overline{x}} - \mathrm{i}|\kappa| \mathrm{e}^{-|\kappa| y^{(0)}}\right), \tag{2.13}$$

$$\begin{aligned}\overline{v}^{(0)} = {} & \frac{\mathrm{e}^{\mathrm{i}\overline{x} + \mathrm{i}\kappa_2 y^{(0)} - \left(\kappa^2 + \kappa_2^2\right)\overline{x}}}{\kappa_2 - \mathrm{i}|\kappa|}\left(\frac{\kappa_2 \beta\left(\kappa_2^2 - \kappa^2\right)}{2\overline{x}\left(\kappa^2 + \kappa_2^2\right)} - \frac{1 + \mathrm{i}\left(\kappa^2 + \kappa_2^2\right)}{(2\overline{x})^{1/2}}\right) + \frac{\mathrm{e}^{\mathrm{i}\overline{x} - |\kappa| y^{(0)}}}{\kappa_2 - \mathrm{i}|\kappa|} \\ & \times \left(-2\mathrm{i}\beta|\kappa|^3 + (2\overline{x})^{-1/2} + \frac{\mathrm{i}|\kappa|\beta}{4\overline{x}}\left(1 + 2|\kappa| y^{(0)}\right)\right) + \frac{|\kappa| \mathrm{e}^{\mathrm{i}\overline{x} - |\kappa| y^{(0)}}}{(2\overline{x})^{1/2}} \int_0^{\overline{x}} g^{(0)}(\check{x}) \mathrm{e}^{-\mathrm{i}\check{x}} \mathrm{d}\check{x},\end{aligned} \tag{2.14}$$

$$\begin{aligned}\overline{w}^{(0)} = {} & \frac{2\mathrm{i}\beta\kappa^2\kappa_2^2\ \mathrm{e}^{\mathrm{i}\overline{x} + \mathrm{i}\kappa_2 y^{(0)} - \left(\kappa^2 + \kappa_2^2\right)\overline{x}}}{(2\overline{x})^{1/2}\left(\kappa_2 - \mathrm{i}|\kappa|\right)\left(\kappa^2 + \kappa_2^2\right)} + \frac{\mathrm{i}\beta\kappa^2 \mathrm{e}^{\mathrm{i}\overline{x} - |\kappa| y^{(0)}}}{\kappa_2 - \mathrm{i}|\kappa|}\left(\frac{1/2 + |\kappa| y^{(0)}}{(2\overline{x})^{1/2}} - 2\kappa^2 (2\overline{x})^{1/2}\right) \\ & + \kappa^2 \mathrm{e}^{\mathrm{i}\overline{x} - |\kappa| y^{(0)}} \int_0^{\overline{x}} g^{(0)}(\check{x}) \mathrm{e}^{-\mathrm{i}\check{x}} \mathrm{d}\check{x},\end{aligned} \tag{2.15}$$

$$\overline{p}^{(0)} = -\frac{\mathrm{i}\beta \mathrm{e}^{i\overline{x}}}{(2\overline{x})^{3/2}(\kappa_2 - \mathrm{i}|\kappa|)}\left(\left(\frac{1}{2} + |\kappa| y^{(0)}\right) \mathrm{e}^{-|\kappa| y^{(0)}} + \frac{2\kappa_2^2\ \mathrm{e}^{\mathrm{i}\kappa_2 y^{(0)} - \left(\kappa^2 + \kappa_2^2\right)\overline{x}}}{\kappa^2 + \kappa_2^2}\right) + g^{(0)}(\overline{x}) \mathrm{e}^{-|\kappa| y^{(0)}} \tag{2.16}$$

and

$$\overline{u} = 0, \tag{2.17}$$

$$\overline{v} = \frac{\mathrm{i}\mathrm{e}^{\mathrm{i}\overline{x}}}{(\kappa_2 - \mathrm{i}|\kappa|)(2\overline{x})^{1/2}}\left(\mathrm{e}^{\mathrm{i}\kappa_2 y^{(0)} - (\kappa^2+\kappa_2^2)\overline{x}} - \mathrm{e}^{-|\kappa|y^{(0)}}\right) + \frac{|\kappa|\mathrm{e}^{i\overline{x}-|\kappa|y^{(0)}}}{(2\overline{x})^{1/2}}\int_0^{\overline{x}} g(\check{x})\mathrm{e}^{-\mathrm{i}\check{x}}\mathrm{d}\check{x}, \tag{2.18}$$

$$\overline{w} = \frac{\mathrm{e}^{\mathrm{i}\overline{x}}}{\kappa_2 - \mathrm{i}|\kappa|}\left(\kappa_2\mathrm{e}^{\mathrm{i}\kappa_2 y^{(0)} - (\kappa^2+\kappa_2^2)\overline{x}} - \mathrm{i}|\kappa|\mathrm{e}^{-|\kappa|y^{(0)}}\right) + \kappa^2\mathrm{e}^{\mathrm{i}\overline{x}-|\kappa|y^{(0)}}\int_0^{\overline{x}} g(\check{x})\mathrm{e}^{-\mathrm{i}\check{x}}\mathrm{d}\check{x}, \tag{2.19}$$

$$\overline{p} = g(\overline{x})\mathrm{e}^{-|\kappa|y^{(0)}}, \tag{2.20}$$

where $g^{(0)}(\overline{x})$ and $g(\overline{x})$ are unknown. Equations (2.17)–(2.20) are also given in Leib *et al.* (1999) as (5.20)–(5.23). The coefficients $\kappa_2/(\kappa_2 - \mathrm{i}|\kappa|)$ and $-\mathrm{i}|\kappa|/(\kappa_2 - \mathrm{i}|\kappa|)$ in (2.19) for $\overline{w}$ are found by imposing two conditions. The first condition is that $\overline{w} \to \exp(\mathrm{i}\overline{x})$ as $\overline{x} \to 0^+$ because this is the behaviour of the spanwise velocity component as the free stream and the leading edge are approached (see (4.12) in Leib *et al.* 1999, p. 177). The second condition is that $\overline{v}$ must be bounded as $\overline{x} \to 0^+$ to match the boundary-layer initial condition given by (4.13) in Leib *et al.* (1999, p. 177), i.e. $\overline{v} \to (\eta^2 F'' - 3\eta F' - F)/4$. Note that the outer behaviour for the spanwise velocity component and the upstream behaviour of the wall-normal velocity component for the boundary-layer case ($\kappa = 0$, studied by Leib *et al.* 1999 and given at p. 177 of their work) may be used in the boundary-region case when $\overline{x} \to 0^+$ because in this limit the spanwise diffusion and the upward displacement effects on the gust are negligible. It is mathematically interesting to note that the same coefficients are found in (2.13) for $\overline{u}^{(0)}$ by imposing a different condition. For this component, it is required that $\overline{w}^{(0)} \to 0$ as $\kappa \to 0$ for every κ_2 at every $\overline{x}$, namely that in the boundary-layer case there be no pressure disturbance at leading order to generate a spanwise velocity fluctuation in the free stream and within the boundary layer. Similar to $\overline{v}$, the component $\overline{v}^{(0)}$ must match the boundary-layer initial condition as $\overline{x} \to 0^+$ because the gust behaves as if $\kappa = 0$; namely the spanwise viscous dissipation and the upward displacement are negligible. However, $\overline{v}^{(0)}$ is not bounded like $\overline{v}$ as $\overline{x} \to 0^+$, but it grows as $\sim \overline{x}^{-1}$: $\overline{v} \to (\eta(\eta F')' - F)/(4\overline{x})$ ((4.13) in Leib *et al.* 1999). The expressions for the free-stream forcing components, (2.13) for $\overline{u}^{(0)}$ and (2.19) for $\overline{w}$, coincide apart from the integral term in (2.19), due to the spanwise pressure gradient when $\kappa = O(1)$. This term is absent in (2.13) because the streamwise pressure gradient is negligible for low-frequency disturbances.

Equations (2.13) and (2.17) can be applied as Dirichlet boundary conditions as $\eta \to \infty$, whereas (2.14)–(2.16) and (2.18)–(2.20) cannot be employed as such because $g, g^{(0)}$ are unknown. These functions can be eliminated to obtain the boundary conditions

$$\frac{\partial\overline{v}^{(0)}}{\partial\eta} + |\kappa|(2\overline{x})^{1/2}\overline{v}^{(0)} \to \frac{\mathrm{i}\beta\kappa^2\mathrm{e}^{\mathrm{i}\overline{x}-|\kappa|(2\overline{x})^{1/2}\overline{\eta}}}{(\kappa_2 - \mathrm{i}|\kappa|)(2\overline{x})^{1/2}} + \left(\frac{\mathrm{i}\kappa_2\beta\left(\kappa_2^2 - \kappa^2\right)}{(2\overline{x})^{1/2}\left(\kappa^2 + \kappa_2^2\right)} - \mathrm{i} + \kappa^2 + \kappa_2^2\right)\mathrm{e}^{i\overline{x}+\mathrm{i}\kappa_2(2\overline{x})^{1/2}\overline{\eta}-\left(\kappa^2+\kappa_2^2\right)\overline{x}}, \tag{2.21}$$

$$\frac{\partial\overline{w}^{(0)}}{\partial\eta} + |\kappa|(2\overline{x})^{1/2}\overline{w}^{(0)} \to \frac{\mathrm{i}\beta|\kappa|^3\mathrm{e}^{\mathrm{i}\overline{x}-|\kappa|(2\overline{x})^{1/2}\overline{\eta}}}{\kappa_2 - \mathrm{i}|\kappa|} - \frac{2\beta\kappa^2\kappa_2^2\ \mathrm{e}^{\mathrm{i}\overline{x}+\mathrm{i}\kappa_2(2\overline{x})^{1/2}\overline{\eta}-\left(\kappa^2+\kappa_2^2\right)\overline{x}}}{\kappa^2 + \kappa_2^2}, \tag{2.22}$$

$$\frac{\partial\overline{p}^{(0)}}{\partial\eta} + |\kappa|(2\overline{x})^{1/2}\overline{p}^{(0)} \to -\frac{\mathrm{i}\beta|\kappa|\mathrm{e}^{\mathrm{i}\overline{x}-|\kappa|(2\overline{x})^{1/2}\overline{\eta}}}{2\overline{x}(\kappa_2 - \mathrm{i}|\kappa|)} + \frac{\beta\kappa_2^2\ \mathrm{e}^{\mathrm{i}\overline{x}+\mathrm{i}\kappa_2(2\overline{x})^{1/2}\overline{\eta}-(\kappa^2+\kappa_2^2)\overline{x}}}{\overline{x}\left(\kappa^2 + \kappa_2^2\right)} \tag{2.23}$$

and

$$\frac{\partial \overline{v}}{\partial \eta} + |\kappa|(2\overline{x})^{1/2}\overline{v} \to -\mathrm{e}^{\mathrm{i}\overline{x}+\mathrm{i}\kappa_2(2\overline{x})^{1/2}\overline{\eta}-\left(\kappa^2+\kappa_2^2\right)\overline{x}}, \tag{2.24}$$

$$\frac{\partial \overline{w}}{\partial \eta} + |\kappa|(2\overline{x})^{1/2}\overline{w} \to \mathrm{i}\kappa_2(2\overline{x})^{1/2}\mathrm{e}^{\mathrm{i}\overline{x}+\mathrm{i}\kappa_2(2\overline{x})^{1/2}\overline{\eta}-\left(\kappa^2+\kappa_2^2\right)\overline{x}}, \tag{2.25}$$

$$\frac{\partial \overline{p}}{\partial \eta} + |\kappa|(2\overline{x})^{1/2}\overline{p} \to 0, \tag{2.26}$$

as $\eta \to \infty$. For $\{\overline{u}, \overline{v}, \overline{w}, \overline{p}\}$, the spanwise component is balanced by the wall-normal component through continuity and drives the laminar streaks in the core of the boundary layer. The pressure disturbance $\overline{p}$ plays no role. The physical mechanism involved in the formation of the outer portion of the Klebanoff modes, i.e. $\{\overline{u}^{(0)}, \overline{v}^{(0)}, \overline{w}^{(0)}, \overline{p}^{(0)}\}$, is slightly subtler. The wall-normal gradient of the streamwise velocity perturbation in the free stream, mainly caused by the displacement effect due to the boundary-layer growth, generates an unsteady pressure $\overline{p}^{(0)}$. This pressure induces the spanwise velocity component $\overline{w}^{(0)}$ which is balanced by $\overline{u}^{(0)}$ and $\overline{v}^{(0)}$. The velocity components and the pressure fluctuations are therefore all forcing the disturbances inside the boundary layer.

For a two-dimensional gust, the outer boundary conditions simplify to

$$\overline{u}^{(0)} \to \mathrm{e}^{\mathrm{i}\overline{x}+\mathrm{i}\kappa_2(2\overline{x})^{1/2}\overline{\eta}-\kappa_2^2\overline{x}}, \tag{2.27}$$

$$\frac{\partial \overline{v}^{(0)}}{\partial \eta} \to \left(\mathrm{i}\kappa_2\beta(2\overline{x})^{-1/2} - \mathrm{i} + \kappa_2^2\right)\mathrm{e}^{\mathrm{i}\overline{x}+\mathrm{i}\kappa_2(2\overline{x})^{1/2}\overline{\eta}-\kappa_2^2\overline{x}}, \tag{2.28}$$

$$\frac{\partial \overline{p}^{(0)}}{\partial \eta} \to \beta\overline{x}^{-1}\mathrm{e}^{\mathrm{i}\overline{x}+\mathrm{i}\kappa_2(2\overline{x})^{1/2}\overline{\eta}-\kappa_2^2\overline{x}}. \tag{2.29}$$

Note that for the response to a two-dimensional gust the pressure $\overline{p}^{(0)}$ appears in (2.11) and in (2.29) only in its wall-normal derivative $\partial\overline{p}^{(0)}/\partial\eta$, so that its actual value remains undetermined.

2.1.2. *Initial conditions*

The initial conditions for $\{\overline{u}, \overline{v}, \overline{w}, \overline{p}\}$ (see (5.25)–(5.27) in Leib *et al.* 1999, p. 182) are

$$\overline{u} \to 2\overline{x}\tilde{U}_0 + (2\overline{x})^{3/2}\tilde{U}_1,$$

$$\begin{aligned}\overline{v} \to\ & \tilde{V}_0 + (2\overline{x})^{1/2}\tilde{V}_1 + \frac{\mathrm{i}}{(\kappa_2 - \mathrm{i}|\kappa|)(2\overline{x})^{1/2}}\left(\mathrm{e}^{\mathrm{i}\kappa_2(2\overline{x})^{1/2}\overline{\eta}-\left(\kappa^2+\kappa_2^2\right)\overline{x}} - \mathrm{e}^{-|\kappa|(2\overline{x})^{1/2}\overline{\eta}}\right)\\ & - \left(3\beta/4 - \tfrac{1}{2}g_1|\kappa|(2\overline{x})^{1/2}\right)\mathrm{e}^{-|\kappa|(2\overline{x})^{1/2}\overline{\eta}} - \overline{v}_c,\end{aligned}$$

$$\begin{aligned}\overline{w} \to\ & \tilde{W}_0 + (2\overline{x})^{1/2}\tilde{W}_1 + \frac{1}{\kappa_2 - \mathrm{i}|\kappa|}\left(\kappa_2\mathrm{e}^{\mathrm{i}\kappa_2(2\overline{x})^{1/2}\overline{\eta}-\left(\kappa^2+\kappa_2^2\right)\overline{x}} - \mathrm{i}|\kappa|\mathrm{e}^{-|\kappa|(2\overline{x})^{1/2}\overline{\eta}}\right)\\ & - \frac{3\beta|\kappa|}{4}(2\overline{x})^{1/2}\mathrm{e}^{-|\kappa|(2\overline{x})^{1/2}\overline{\eta}} - \overline{w}_c,\end{aligned}$$

where the quantities in capital letters are the first two terms of the power series

$$\{\overline{u}, \overline{v}, \overline{w}, \overline{p}\} = \sum_{n=0}^{\infty}(2\overline{x})^{n/2}\left\{2\overline{x}\tilde{U}_n(\eta),\ \tilde{V}_n(\eta),\ \tilde{W}_n(\eta),\ \frac{\tilde{P}_n(\eta)}{(2\overline{x})^{1/2}}\right\}.$$

The differential equations and boundary conditions satisfied by the terms are found in Appendix B in Leib *et al.* (1999), and the quantities $\overline{v}_c$ and $\overline{w}_c$ indicate the common parts and are given in Appendix C in Leib *et al.* (1999). The conditions for $\{\overline{u}^{(0)}, \overline{v}^{(0)}, \overline{w}^{(0)}, \overline{p}^{(0)}\}$ are determined by a similar regular perturbation to find a power series for $\eta = O(1)$ and $\overline{x} \ll 1$:

$$\{\overline{u}^{(0)}, \overline{v}^{(0)}, \overline{w}^{(0)}, \overline{p}^{(0)}\} = \sum_{n=0}^{\infty} (2\overline{x})^{n/2} \left\{ U_n(\eta), \frac{V_n(\eta)}{2\overline{x}}, \frac{W_n(\eta)}{(2\overline{x})^{1/2}}, \frac{P_n(\eta)}{(2\overline{x})^{3/2}} \right\}. \tag{2.30}$$

The equations governing the power series terms and the boundary conditions are found in Appendix A. The upstream perturbation profiles for the LUBR equations are obtained by constructing a composite solution that is uniformly valid for all values of η. This is done by using the additive rule, which involves adding the power series (2.30) (which are valid for $\eta = O(1)$) and the small-$\overline{x}$ limit form of expressions (2.13)–(2.16) (which are valid where $y^{(0)} = O(1)$) and subtracting their common part. Note that as the boundary-region equations (2.9)–(2.12) are parabolic in nature, the streamwise pressure gradient is negligible at leading order, which implies that an initial condition for the pressure disturbance is not needed to start the numerical integration. The series expression for the pressure disturbance in (2.30) has however been useful to check the numerical results at small $\overline{x}$ locations. The reader is referred to Appendix B for the initial conditions. Note that the asymptotic solution for $\kappa, \kappa_2 \ll 1$ as $\overline{x} \to \infty$, studied by Leib *et al.* (1999, pp. 177–179), may not be used as initial condition for the boundary-region equations. In that case, the disturbances are exponentially small in the core of the boundary layer and are confined near the free stream. This behaviour is in marked contrast with the one of the streaks when $\overline{x} \ll 1$, which show a peak in the core of the boundary layer and vanish in the outer portion (see Choudhari 1996).

2.2. *Receptivity to vorticity disturbances interacting with wall inhomogeneities*

The mathematical formulation for the TS-wave generation by the interaction of the free-stream-induced vorticity fluctuations with localized wall inhomogeneities at a distance $x^* = l^*$ is presented in this section. A schematic of the physical mechanism for the wall-roughness case is shown in figure 3. The FRN approach pioneered by Choudhari & Streett (1992) for free-stream acoustic forcing is adopted. The reader should refer to Choudhari (1994*a*,*b*, 1996) for further details. The receptivity problem is formulated for the general three-dimensional case with $k_3 \neq 0$, although the calculations in § 4.2 are carried out for a two-dimensional free-stream gust.

We consider localized surface disturbances of two types, wall roughness and wall suction. Similar to the vorticity flow induced from the free stream, the mean flow produced by the wall perturbation is assumed small compared with the unperturbed Blasius flow, which implies that the equations can be linearized. In the wall-roughness case, the maximum height of the roughness element, $h^*_{w,m} = \max_x (h^*_w(x^*))$, is therefore taken as small compared with a measure of the wall-normal length scale of the Blasius flow in the proximity of the wall. The asymptotic triple-deck theory (Sobey 2001) shows that the condition for linearization is that the maximum height of the roughness must be much smaller than the inner layer of the multiple-scale interaction, namely $h^*_{w,m}/x^* \ll Re_x^{-5/8}$, where $Re_x = x^* U_\infty/\nu$. In receptivity studies, the distances are usually scaled by the displacement thickness

$$\delta^*_d = d\sqrt{x^*\nu/U_\infty} = dx^* Re_x^{-1/2}, \quad d = 1.72078\ldots,$$

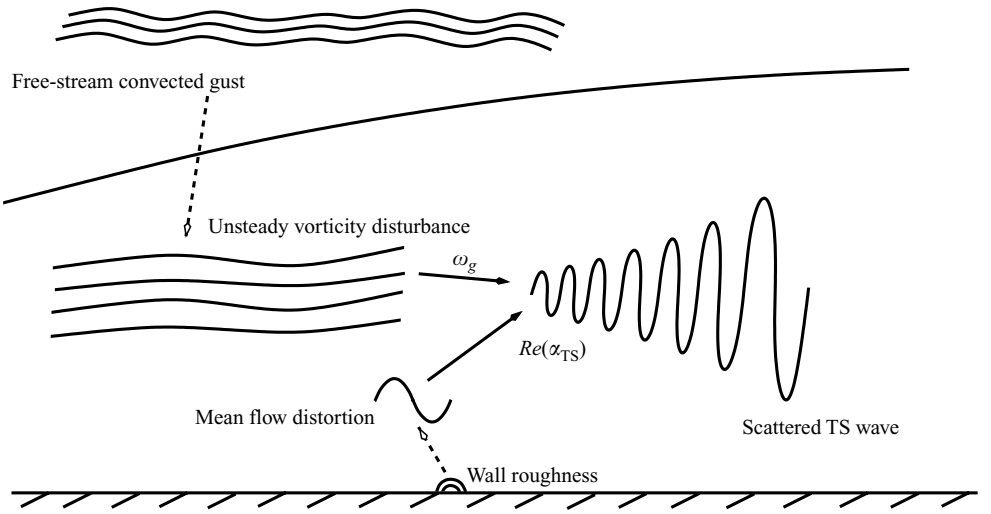

FIGURE 3. Schematic of physical mechanism of generation of TS waves by unsteady vorticity disturbances interacting with localized wall roughness. The dashed arrows indicate the linear responses from the free stream and the wall, while the solid arrows denote the nonlinear interaction between the vorticity disturbance and the mean flow distortion which causes the TS-wave scattering. The frequency ω_g is extracted from the free-stream gust, while the streamwise wavenumber $\mathrm{Re}(\alpha_{TS})$ is provided by the wall inhomogeneity.

at $x^* = l^*$, so that the condition for linearization is $h^*_{w,m}/\delta^*_d \ll Re_x^{-1/8}$. The asymptotically small parameter $\epsilon^r_w \equiv h^*_{w,m}/\delta^*_d$ is defined. For wall suction, the maximum steady suction velocity, $v^*_{s,m} = \max_x (v^*_s(x^*))$, is assumed much smaller than U_∞, and we define $\epsilon^s_w \equiv v^*_{s,m}/U_\infty \ll 1$. The scaled wall perturbations can be expressed as $h_w(X) = \epsilon^r_w H^r_w(X)$ and $v_s(X) = \epsilon^s_w H^s_w(X)$, where $H^j_w(X) = O(1)$ $(j = r, s)$ and $X = x^*/\delta^*_d$.

The downstream Reynolds number can also be defined on δ^*_d as $Re_\delta = \delta^*_d U_\infty/\nu = d\sqrt{Re_x}$. The frequency is scaled as follows:

$$f \equiv \frac{\omega^* \nu}{U^2_\infty} \quad \text{or} \quad \omega_g \equiv \frac{\omega^* \delta^*_d}{U_\infty} = f Re_\delta.$$

The spanwise wavenumber of the gust and of the TS wave becomes

$$\beta_g \equiv \frac{2\pi\delta^*_d}{\lambda^*_z} = \frac{\omega_g k_3}{k_1},$$

and the scaled downstream distance for the vorticity response can be expressed as

$$\overline{x} = f Re_x. \tag{2.31}$$

The velocity field in the boundary layer is

$$\begin{aligned}\{u, v, w\}(X, Y, Z, T) = {} & \{U(Y), 0, 0\} + \epsilon^j_w \{U_w(X, Y), V_w(X, Y)\} \\ & + \epsilon_g \{U_g(Y), V_g(Y), W_g(Y)\} \mathrm{e}^{\mathrm{i}\alpha_g X + \mathrm{i}\beta_g Z - \mathrm{i}\omega_g T} + \epsilon^j_w \epsilon_g \\ & \times \{U_{w,g}(X, Y), V_{w,g}(X, Y), W_{w,g}(X, Y)\} \mathrm{e}^{\mathrm{i}\beta_g Z - \mathrm{i}\omega_g T} + \ldots, \end{aligned} \tag{2.32}$$

where $\alpha_g = \omega_g$. The first term on the right is the Blasius solution. The quasi-parallel flow assumption is adopted; i.e. the wall-normal velocity of the Blasius flow is assumed small compared with the streamwise velocity. The quantities with subscript w are the steady flow distortion induced by the wall roughness or wall suction, and

the quantities with subscript g are the unsteady vorticity disturbances induced by the free-stream perturbations. The quantities with subscript w, g indicate the scattered TS wave, which is produced by the nonlinear interaction between the two previous perturbations. Similar to X, the wall-normal and spanwise coordinates, Y, Z, are scaled by δ_d^* and the time T by δ_d^*/U_∞. The wall-normal coordinate Y is related to η, the coordinate used in the Klebanoff modes analysis: $Y = \sqrt{2}\eta/d$.

The boundary-layer vorticity response is

$$U_g(Y)\mathrm{e}^{\mathrm{i}\alpha_g X} \approx \overline{u}_0, \quad V_g(Y)\mathrm{e}^{\mathrm{i}\alpha_g X} \approx \left(\frac{2\overline{x}k_1}{R_\lambda}\right)^{1/2}\overline{v}_0, \quad W_g(Y)\mathrm{e}^{\mathrm{i}\alpha_g X} \approx \overline{w}_0, \tag{2.33}$$

where $\overline{u}_0, \overline{v}_0, \overline{w}_0$, given in (2.7) and (2.8), are composed of both the components studied by Leib *et al.* (1999), which are dominant in the core of the boundary layer, and the components $\{\overline{u}^{(0)}, \overline{v}^{(0)}, \overline{w}^{(0)}, \overline{p}^{(0)}\}$, which are the relevant ones in the outer portion of the boundary layer. As in Choudhari (1996), it is assumed that the vorticity response locally presents a streamwise modulation with wavenumber α_g, which is $\alpha_g = \omega_g$ for a convected gust. We therefore expect the localized wall perturbations to be at a downstream location at which the Klebanoff modes relax to the streamwise behaviour of the free-stream convected gust. Expression (2.33) is a good approximation because the vorticity response evolves on a streamwise scale $O(\lambda_x^*)$, which is much larger than the streamwise wavelength of the TS waves (assumed to be of the same order of δ_d^*) and much shorter than the scale of the mean boundary layer, i.e. the distance from the leading edge. Furthermore, following the results by Wu (2001*a*,*b*) based on a rigorous asymptotic analysis for two-dimensional, low-frequency disturbances, we adopt the 'inner approximation'; namely we neglect the effect of the exponentially decaying (along y) part of the free-stream gust.

An equation of motion for the wall-normal velocity component is obtained from the Navier–Stokes equations by taking the divergence of the momentum equations and by using the continuity equation to eliminate the pressure (see Kim, Moin & Moser 1987 for the derivation, although for the stability analysis the nonlinear terms are neglected). Solution (2.32) is substituted into this equation, and terms $O(\epsilon_w^j)$ and $O(\epsilon_w^j\epsilon_g)$ are collected. The velocity components of the disturbance are Fourier transformed along the X direction because the coefficients of the equation are independent of this coordinate. The homogeneous Orr–Sommerfeld equation for the Fourier-transformed wall-normal velocity component $\overline{V}_w$ of the mean flow distortion is obtained by collecting $O(\epsilon_w^j)$ terms:

$$\mathscr{L}_{OS}(\overline{V}_w) = 0, \quad \mathscr{L}_{OS} = \mathrm{i}(\alpha U - \omega_g)(D^2 - \alpha^2) - \mathrm{i}\alpha U_{YY} - \frac{1}{Re_\delta}(D^2 - \alpha^2)^2,$$

where D and the subscript Y indicate differentiation with respect to the wall-normal coordinate. The following boundary conditions apply:

$$\overline{V}_w, \overline{V}_{wY} \to 0 \quad \text{as } Y \to \infty,$$
$$\overline{V}_w = 0, \quad \overline{V}_{wY} = \mathrm{i}\alpha U_Y(0)\overline{H}_w^r(\alpha), \quad \text{at } Y = 0 \text{ for wall roughness},$$

and

$$\overline{V}_w = \overline{H}_w^s(\alpha), \ \overline{V}_{wY} = 0, \ \text{at } Y = 0 \text{ for wall suction},$$

where the no-slip boundary condition at the wall roughness ($Y = h_w(X)$) has been shifted to $Y = 0$ through a Taylor expansion in Y. The streamwise velocity can be computed by the continuity equation to obtain $\overline{U}_w = \mathrm{i}\overline{V}_{wY}/\alpha$. Note that the calculations above for the mean flow distortion are carried out at the complex

wavenumber of the instability wave, $\alpha = \alpha_{TS}(\omega_g, Re_\delta)$, which is computed from the stability calculations based on the homogeneous Orr–Sommerfeld equation.

By collecting $O(\epsilon_w^j \epsilon_g)$ terms, the inhomogeneous Orr–Sommerfeld equation for the wall-normal velocity of the TS wave is found,

$$\begin{aligned}\mathscr{L}_{OS}(\overline{V}_{w,g}) = {} & \mathrm{i}\alpha_g^3 \overline{U}_w \overline{V}_g + \mathrm{i}\alpha_w^3 \overline{V}_w \overline{U}_g - \mathrm{i}\alpha_g \overline{U}_w \overline{V}_{gYY} - \mathrm{i}\alpha_w \overline{V}_{wYY} \overline{U}_g \\ & + \mathrm{i}\alpha_g \beta^2 \overline{U}_w \overline{V}_g + \alpha_g^2 \overline{V}_w \overline{V}_{gY} + \alpha_w^2 \overline{V}_{wY} \overline{V}_g - \overline{V}_w \overline{V}_{gYYY} - \overline{V}_{wYYY} \overline{V}_g \\ & + \beta^2 \overline{V}_w \overline{V}_{gY} + 2\mathrm{i}\alpha_w \alpha_g^2 \overline{U}_w \overline{V}_g + 2\mathrm{i}\alpha_w^2 \alpha_g \overline{V}_w \overline{U}_g - 2\alpha_g \alpha_w (\overline{U}_w \overline{U}_{gY} + \overline{U}_{wY} \overline{U}_g) \\ & + \mathrm{i}\alpha_w \alpha_g (\alpha_g \overline{V}_w \overline{U}_g + \alpha_w \overline{U}_w \overline{V}_g) + \mathrm{i}(\alpha_w \overline{V}_w \overline{U}_{gYY} + \alpha_g \overline{U}_{wYY} \overline{V}_g) \\ & + \mathrm{i}\alpha_w \beta^2 \overline{V}_w \overline{U}_g + 2\alpha_w \alpha_g (\overline{V}_w \overline{V}_{gY} + \overline{V}_{wY} \overline{V}_g) + \left(\alpha_g^2 \overline{V}_{wY} \overline{V}_g + \alpha_w^2 \overline{V}_w \overline{V}_{gY}\right) \\ & - \overline{V}_{wY} \overline{V}_{gYY} - \overline{V}_{wYY} \overline{V}_{gY} + \beta^2 \overline{V}_{wY} \overline{V}_g, \end{aligned} \tag{2.34}$$

which is subject to the following boundary conditions:

$$\begin{aligned} \overline{V}_{w,g} = 0, \quad \overline{V}_{w,gY} = \mathrm{i}\alpha_w \overline{U}_{gY} \overline{H}_w(\alpha_w), \quad \text{at } Y = 0, \quad \text{for wall roughness,} \\ \overline{V}_{w,g} = 0, \quad \overline{V}_{w,gY} = 0, \quad \text{at } Y = 0 \quad \text{for wall suction,} \end{aligned} \tag{2.35}$$

and

$$\overline{V}_{w,g}, \overline{V}_{w,gY} \to 0 \text{ as } Y \to \infty.$$

The streamwise wavenumber $\alpha_w \equiv \alpha - \alpha_g$ is defined. The source term on the right-hand side of (2.34) synthesizes the nonlinear interaction between the free-stream vorticity flow and the mean flow distortion.

The objective is to determine the amplitude of the streamwise velocity component of the TS wave. This is usually the quantity of interest in receptivity studies because it is often measured in experiments. It can be expressed as

$$U_{w,g}(X, Y, Z, T) = \epsilon_w^j \overline{H}_w^j(\alpha_{TS} - \alpha_g) \epsilon_g \Lambda_u(\omega_g, Re_\delta) E_u(Y; \omega_g, Re_\delta) \mathrm{e}^{\mathrm{i}(\alpha_{TS} X + \beta_g Z - \omega_g T)},$$

where $E_u(Y; \omega_g, Re_\delta)$ indicates the eigenfunction of the streamwise velocity component of the instability wave. It is scaled so that the maximum of its absolute value is unity. Also in the above equation, $\overline{H}_w^j$ is the Fourier transform of the X distribution of the wall perturbation. The quantity $\Lambda_u(\omega_g, Re_\delta)$ is the efficiency function, and it depends on the types of free-stream disturbance and surface inhomogeneities, but it is independent of the actual shape of the wall disturbance. This represents a valuable asset of receptivity studies, as discussed in Choudhari & Streett (1992). The product $\Lambda_u E_u$ is evaluated by the residue contribution of the simple pole at the TS-wave eigenvalue α_{TS}, calculated by solving numerically the homogeneous Orr–Sommerfeld stability problem. The solution is

$$\Lambda_u E_u = \frac{\sqrt{2\pi}\mathrm{i}}{\overline{H}_w^j(\alpha_{TS} - \alpha_g) \left.\dfrac{\partial\left(\overline{U}_{w,g}{}^{-1}\right)}{\partial\alpha}\right|_{\alpha=\alpha_{TS}}},$$

from which $|\Lambda_u|$ is found.

3. Numerical procedures

The mean-flow equation (2.6) is decomposed into three ordinary differential equations, which are solved by a second-order, implicit finite-difference scheme. The nonlinear system is solved by Newton–Raphson iteration (Cebeci 2002).

3.1. *Solution of the LUBR equations*

The LUBR equations (2.9)–(2.12) are parabolic in the $\bar{x}$ direction and elliptic in the z direction, so that they can be solved by marching downstream by applying the initial conditions (B1)–(B4) and (5.25)–(5.27) in Leib *et al.* (1999, p. 182), the outer boundary conditions (2.13), (2.17), (2.21)–(2.23) and (2.24)–(2.26) and the no-slip condition at the wall. A second-order, implicit finite-difference scheme which is central in η and backward in $\bar{x}$ is employed for the computation of $\{\bar{u}, \bar{v}, \bar{w}, \bar{p}\}$. The discretization scheme along $\bar{x}$ is increased to third order for the computation of $\{\bar{u}^{(0)}, \bar{v}^{(0)}, \bar{w}^{(0)}, \bar{p}^{(0)}\}$ because higher accuracy is required near the leading edge as $\bar{v}^{(0)}, \bar{w}^{(0)}$ are singular as $\bar{x} \to 0^+$ (see (2.30)). The pressure terms are computed on a grid staggered in the η direction with respect to the grid for the velocity components with the purpose of avoiding the pressure decoupling phenomenon. This undesired effect occurs if the grid for the pressure coincides with the grid for the velocity components. The pressure at the wall needs not be specified; its value is calculated *a posteriori* by solving the z-momentum equation at $\eta = 0$. The outer mixed boundary conditions (2.21)–(2.23) and (2.24)–(2.26) are applied by a second-order finite-difference approximation. The linear system is solved by a standard block-elimination algorithm, described in Cebeci (2002, pp. 260–264). A uniform grid with a typical mesh size of $\Delta\eta = 0.05$ is used, and the domain extends to $\eta = 30$.

The numerical implementation of the initial conditions for $\bar{v}^{(0)}, \bar{w}^{(0)}$ requires special attention because of their singular behaviour as $\bar{x} \to 0^+$. If the calculations are started at a too small $\bar{x}_0$ value, the streamwise gradients $\partial\bar{v}^{(0)}/\partial\bar{x}, \partial\bar{w}^{(0)}/\partial\bar{x}$ are too large and the finite-difference scheme may not approximate accurately the analytic expression for the initial conditions (B1) and (B2). On the other hand, calculations must be started at a small enough $\bar{x}_0$ for the initial conditions to be valid. The integration step $\Delta\bar{x}$ must be kept small during the initial iterations, while it can be increased as the streamwise gradients decrease downstream. The values of $\bar{x}_0$ and of the initial $\Delta\bar{x}$ are found iteratively by minimizing the error between the numerical and analytical expressions for $\partial\bar{v}^{(0)}/\partial\bar{x}, \partial\bar{w}^{(0)}/\partial\bar{x}$ during the initial numerical calculations. For $\kappa = \kappa_2 = 1$, $\bar{x}_0 \approx 10^{-3}$, and $\Delta\bar{x} \approx 10^{-4}$ near the leading edge ($\bar{x} < 0.01$), and $\Delta\bar{x} \approx 10^{-3}$ further downstream. This problem is not encountered for $\bar{v}, \bar{w}$ because these components are bounded for small $\bar{x}$, so that the calculations may be started from any small non-zero $\bar{x}$ value. The pressure terms $\bar{p}, \bar{p}^{(0)}$ are also singular in this limit, but their initial conditions are not needed to initiate the numerical calculations because the streamwise pressure gradient term is absent in the LUBR equations. Expressions (B4) and (4.16) in Ricco & Wu (2007, p. 111) are only used to verify the correctness of the pressure profiles during the initial integration steps. As further checks, the solutions of the LUBR equations for vanishingly small values of κ and κ_2 are successfully compared with the solutions to the boundary-layer equations (see Leib *et al.* 1999, p. 176), obtained by a separate code which employs the Keller-box method (Cebeci 2002), and with the results by Choudhari (1996). The solutions of the LUBR equations for $\{\bar{u}, \bar{v}, \bar{w}, \bar{p}\}$ with $\kappa, \kappa_2 = O(1)$ match the ones by Leib *et al.* (1999).

3.2. *Solution of the stability and receptivity equations*

The Orr–Sommerfeld stability equation has been solved by two methods: a fourth-order explicit Runge–Kutta scheme which employs the compound matrix method, and a second-order fully implicit finite-difference method. The solutions of the two methods show excellent agreement. The reader should refer to the papers by Ng & Reid (1979), Davey (1982), Sengupta (1992), Allen & Bridges (2002, 2003*a*,*b*) and

Sengupta & Subbaiah (2006) for details on the compound matrix method used to cure the stiffness-related problems when an explicit algorithm, such as the Runge–Kutta method, is employed. The implicit method is described in Malik (1990). It is a local method in that an initial guess for the eigenvalue is needed and an iteration process leads to the correct solution. The receptivity problem, where the Orr–Sommerfeld equation is inhomogeneous with respect to both the boundary conditions and the nonlinear forcing term, has been solved by the implicit method.

4. Results

4.1. *Boundary-layer vorticity disturbances*

4.1.1. *Response to a two-dimensional free-stream gust*

The boundary-layer disturbance induced by a two-dimensional gust is first investigated. The flow within the boundary layer is also two-dimensional, with velocity components $\overline{u}^{(0)}$ and $\overline{v}^{(0)}$ and pressure $\overline{p}^{(0)}$. The case with a wall-normal wavelength which is long compared with the boundary-layer thickness ($\kappa_2 \to 0$ at $\overline{x} = O(1)$) was first studied by Choudhari (1996) by the unsteady boundary-layer equations (see figure 2 at p. 10 in his paper). Also, $\theta_g = 0$, so that $\hat{u}_1^{\infty} = 0$, $\hat{u}_2^{\infty} = 1$, which represent a simplified gust whose vector is oriented along the y axis. Equation (2.27) simplifies to $\overline{u}^{(0)} \to \exp(\mathrm{i}\overline{x})$, and the amplitude of $\overline{u}^{(0)}$ in the free stream remains equal to unity because the effects of viscous dissipation are negligible. Choudhari (1996) found that this component moves upward towards the free stream and eventually becomes exponentially small in the core of the boundary layer. It confines itself in the so-called edge layer, located in the outer portion of the boundary layer, for which an analytical solution can be found (see Leib *et al.* 1999; Wu 2001*b*).

We consider the boundary-layer response to two-dimensional gusts with wall-normal wavelength comparable with the boundary-layer thickness, i.e. $\kappa = 0$, $\kappa_2 = 1$ and $\kappa = 0$, $\kappa_2 = 2$. (Note that hereinafter the notation $\kappa = 0$ actually indicates $\kappa \ll 1$. A null value cannot be assigned to κ because this quantity appears at the denominator in the initial conditions for the pressure component (B4) and in (A13). A value of $\kappa = 10^{-5}$ was assigned, and the results have been shown to be independent of κ in this limit.) Figure 4 for $\kappa_2 = 1$ and figure 6(*a*) for $\kappa_2 = 2$ show that the amplitude of the streamwise velocity component $\overline{u}^{(0)}$ decays at a faster rate in the free stream than in the core of the boundary layer. The disparity between $|\overline{u}^{(0)}|$ in the free stream and within the boundary layer amplifies as κ_2 increases. The $|\overline{u}^{(0)}|$ peak within the boundary layer remains at almost the same wall-normal location, $\eta \approx 2.2$, when $\kappa_2 = 1$, but when $\kappa_2 = 2$ it moves closer to the wall from $\eta \approx 2.2$ at $\overline{x} \approx 0$ to $\eta \approx 1.8$ at $\overline{x} = 1.0$. If the streamwise velocity is rescaled by the amplitude of its local free-stream value (as is done in receptivity studies), the profile for $\kappa_2 = O(1)$ is significantly different from the case $\kappa_2 = 0$ (shown in figure 2 in Choudhari 1996) because of the presence of the peak in the core of the boundary layer; κ_2 is thus expected to produce a marked effect on the efficiency function of the TS wave, which depends strongly on the shape of the streamwise velocity signature (see § 4.2). The edge-layer entrainment of the disturbances does not occur when $\kappa_2 = O(1)$, similarly to the response to a three-dimensional free-stream gust when $\kappa, \kappa_2 = O(1)$ (see Leib *et al.* 1999; Ricco & Wu 2007).

Figures 5 and 6(*b*) display the amplitude of the wall-normal velocity component $\overline{v}^{(0)}$ at different $\overline{x}$ locations for $\kappa_2 = 1$ and $\kappa_2 = 2$, respectively. The peak of $|\overline{v}^{(0)}|$ occurs at almost the same wall-normal location of $|\overline{u}^{(0)}|$, $\eta \approx 2$. The fluctuations within the

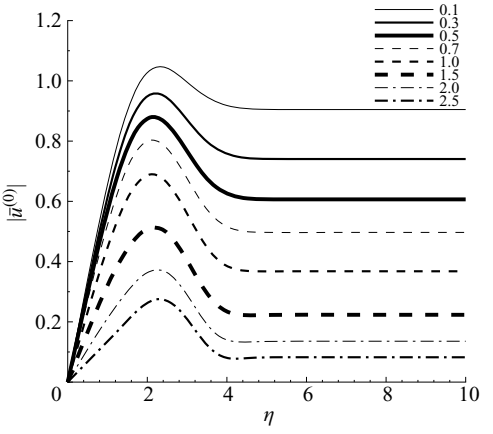

FIGURE 4. Amplitude of streamwise $\overline{u}^{(0)}$ velocity profiles for $\kappa = 0$ and $\kappa_2 = 1$ at different $\overline{x}$ locations.

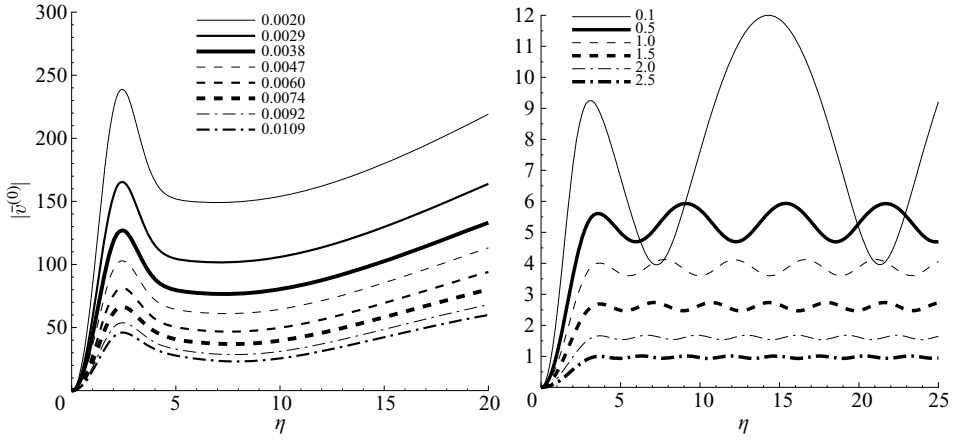

FIGURE 5. Amplitude of wall-normal $\overline{v}^{(0)}$ velocity profiles for $\kappa = 0$ and $\kappa_2 = 1$ at different $\overline{x}$ locations.

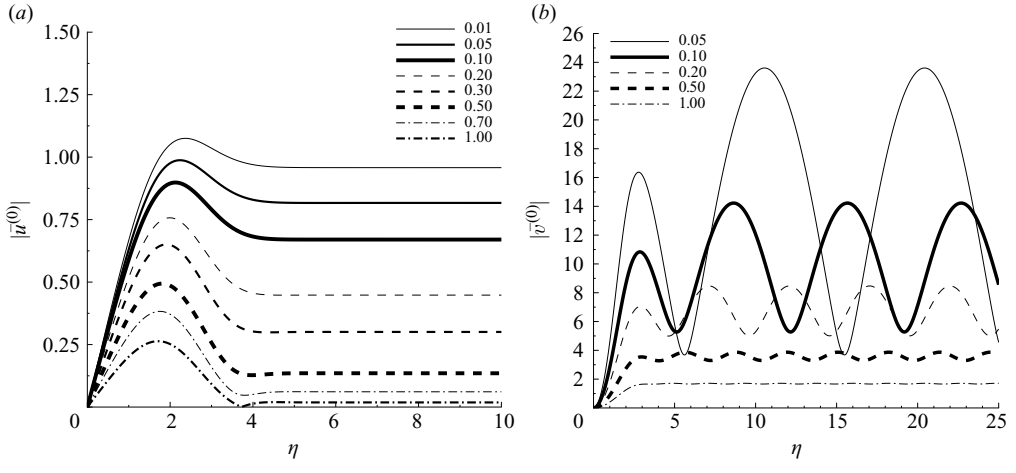

FIGURE 6. Amplitude of (*a*) streamwise $\overline{u}^{(0)}$ and (*b*) wall-normal $\overline{v}^{(0)}$ velocity profiles for $\kappa = 0$ and $\kappa_2 = 2$ at different $\overline{x}$ locations.

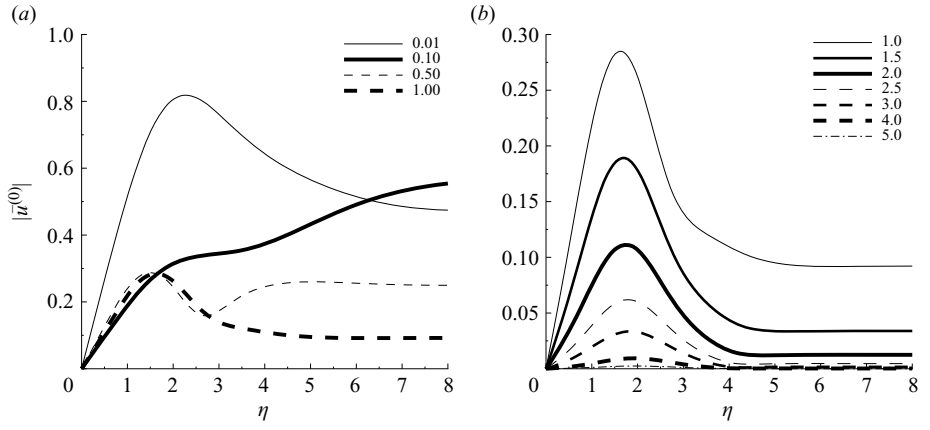

FIGURE 7. Amplitude of streamwise $\overline{u}_0$ velocity profiles for $\kappa = \kappa_2 = 1$, $k_1 = 0.1$, $\hat{u}_3^\infty = -0.2$ at (*a*) $\overline{x} \leqslant 1$ and (*b*) $\overline{x} \geqslant 1$.

boundary layer and in the free stream decay at almost the same rate. This indicates that the mean flow shear acts primarily on the streamwise component, similarly to the three-dimensional case, where the lift-up mechanism is observed (Ellingsen & Palm 1975; Landahl 1980). Downstream of $\overline{x} \approx 0.02$, the profiles show a wavy modulation in the free stream, whose amplitude and wavelength decrease slowly as the flow develops downstream. As expected, the rate of decay is stronger when $\kappa_2 = 2$. The free-stream waviness behaviour is not observed when $\kappa_2 = 0$, for which the profiles vary little from the distribution at $\overline{x} \ll 1$ (Choudhari 1996).

If the experimental work by Dietz (1999, where the response to long-λ_y^* gusts was studied, i.e. $\kappa_2 \approx 0$) were to be extended to investigate the effects of a viscously dissipated and displaced free-stream fluctuation, a gust with a wall-normal wavelength of about 1 mm would have to be generated. This would be of the same order of magnitude of the boundary-layer thickness (less than 2 mm). The non-dimensional wall-normal wavenumber would be $\kappa_2 \approx 1$, as suggested by the asymptotic arguments in § 2.1.

4.1.2. *Response to a three-dimensional free-stream gust: the Klebanoff modes*

In this section, the evolution of boundary-layer disturbances induced by a three-dimensional gust is studied. As the flow is now three-dimensional, we consider the full disturbance solution $\{\overline{u}_0, \overline{v}_0, \overline{w}_0, \overline{p}_0\}$, given in (2.8). The flow parameters are $\kappa = \kappa_2 = 1$, $k_1 = 0.1$ and $\hat{u}_3^\infty = -0.2$. A small value for k_1 was chosen to satisfy the asymptotic condition $k_1 \ll 1$. It was not taken as extremely small in order to investigate the importance of second-order effects and of the vorticity signature in the outer part of the boundary layer. From the condition that the amplitude of the gust vector is unity (2.1) and from the continuity equation (2.2), it follows that $k_2 = 2\pi$, $\hat{u}_1^\infty \approx 0.96$, $\hat{u}_2^\infty \approx 0.18$ and $R_\lambda \approx 394.8$.

Figure 7 shows the amplitude of the streamwise velocity component at different $\overline{x}$ locations, and figure 8 shows the relative importance of the amplitude of the two components of $|\overline{u}_0|$, $|C^{(0)}\overline{u}^{(0)}|$, $|(k_3/k_1)C\overline{u}|$ at $\overline{x} = 0.5, 1.0$. For this frequency k_1, we note the importance of including the component proportional to $\overline{u}^{(0)}$. It has a magnitude comparable with the component proportional to $\overline{u}$ for $\overline{x} \leqslant 1$, is dominant in the outer portion of the boundary layer and matches the streamwise component of the

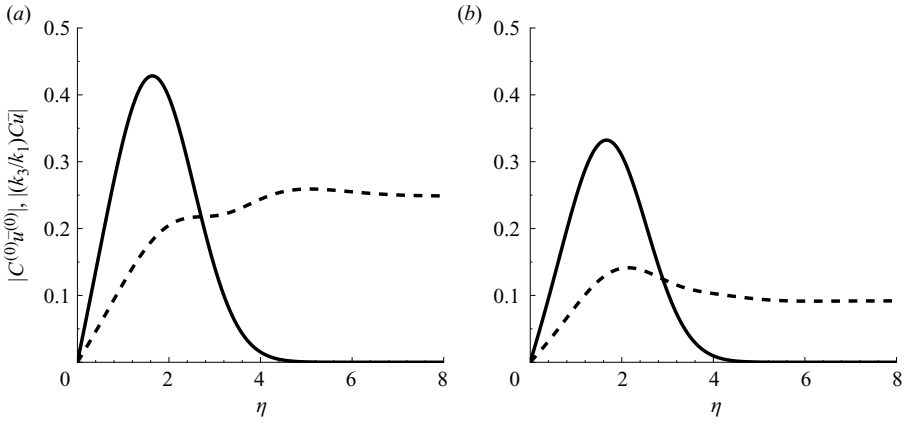

FIGURE 8. Amplitude of streamwise velocity profiles $|C^{(0)}\overline{u}^{(0)}|$ (dashed lines) and $|(k_3/k_1)C\overline{u}|$ (solid lines) for $\kappa = \kappa_2 = 1$, $k_1 = 0.1$, $\hat{u}_3^{\infty} = -0.2$ at (*a*) $\overline{x} = 0.5$ and (*b*) at $\overline{x} = 1.0$.

free-stream gust. The typical profile of the Klebanoff modes appears downstream of this location, with the $\overline{u}$ component playing a leading role in the core of the boundary layer, while $\overline{u}^{(0)}$ becomes gradually less important. As will be verified in § 4.1.3 when the numerical results are compared successfully with experimental data, the inclusion of the $\overline{u}^{(0)}$ component gives a more realistic representation of the Klebanoff mode shape than if only $\overline{u}$ is considered or if the streaks are described by other theories, which allow for the streamwise velocity component to vanish as the free stream is approached. One theory is for example the one by Taylor (1939), who has described the streaks by a small spanwise perturbation of the mean boundary-layer thickness, so that $u \sim \eta F''$.

The disturbance is eventually damped by viscous effects both inside the viscous region and in the free stream, where the dissipating effects of both the wall-normal and the spanwise length scales are at work. The entrainment of disturbance in the outer portion of the boundary layer, in the so-called edge layer, does not occur, being a phenomenon solely restricted to gusts with small κ values (see Choudhari 1996; Leib *et al.* 1999).

The wall-normal and spanwise velocity profiles, respectively shown in figure 9(*a*,*b*), do not present the growth in the core of the boundary layer displayed by the streamwise component, being significantly damped by viscous effects. The free-stream wavy modulation of $|\overline{v}^{(0)}|$ which occurs when $\kappa = 0$, $\kappa_2 = O(1)$ (see figures 5 and 6*b*), is absent when $\kappa = \kappa_2 = 1$. The amplitude of pressure $\overline{p}_0$, shown in figure 10, bears some resemblance with the root mean square (r.m.s.) profile of the pressure fluctuations in a turbulent boundary layer (see Schewe 1983 and Tsuji *et al.* 2007 for experimental results and Spalart 1988 for numerical results), although in this latter case the peak occurs closer to the wall. The local maximum of $|\overline{p}_0|$ in the core of the boundary layer corresponds to the peak of $|\overline{u}_0|$.

The boundary-region solution $\{\overline{u}^{(0)}, \overline{v}^{(0)}, \overline{w}^{(0)}, \overline{p}^{(0)}\}$ can be expressed through an asymptotic solution, $\overline{u}^{(0)} = \hat{u}^{(0)}(\kappa^2\overline{x}, \eta; \kappa_2/\kappa)$, $\{\overline{v}^{(0)}, \overline{w}^{(0)}, \overline{p}^{(0)}\} = \kappa^2\{\hat{v}^{(0)}, \hat{w}^{(0)}, \hat{p}^{(0)}\}(\kappa^2\overline{x}, \eta; \kappa_2/\kappa)$ in the limit $\kappa \to \infty$, $\kappa_2/\kappa = O(1)$. The scaled quantities $\{\hat{u}^{(0)}, \hat{v}^{(0)}, \hat{w}^{(0)}, \hat{p}^{(0)}\}$ satisfy the steady boundary-region equations. This scaling is verified numerically in figure 11, where the profiles tend to collapse on one another as κ grows.

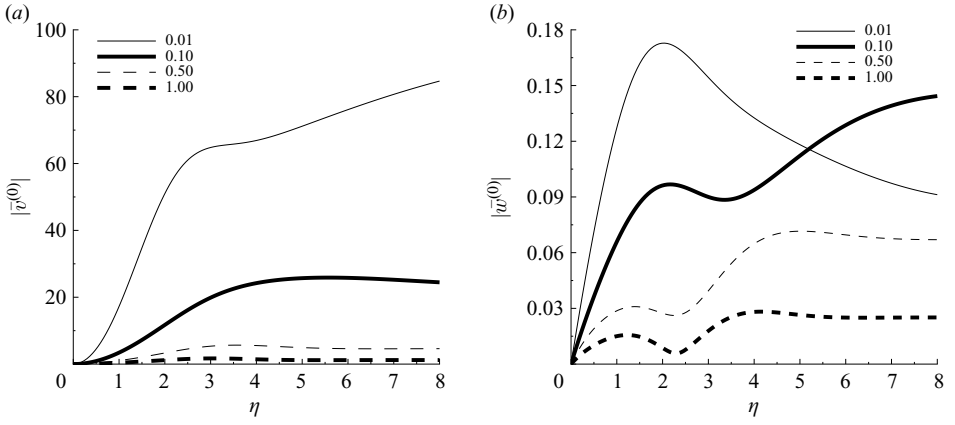

FIGURE 9. Amplitude of (*a*) wall-normal $\overline{v}_0$ and (*b*) spanwise $\overline{w}_0$ velocity profiles for $\kappa = \kappa_2 = 1$, $k_1 = 0.1$, $\hat{u}_3^{\infty} = -0.2$ at different $\overline{x}$ locations.

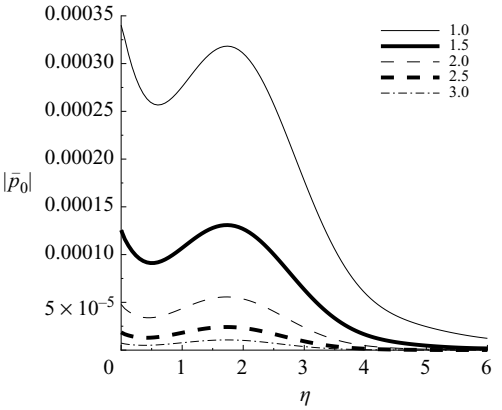

FIGURE 10. Amplitude of pressure $\overline{p}_0$ profiles for $\kappa = \kappa_2 = 1$, $k_1 = 0.1$, $\hat{u}_3^{\infty} = -0.2$ at different $\overline{x}$ locations.

4.1.3. *Comparison with experimental data by Westin* et al. *(1994)*

This section presents comparisons between our numerical calculations and the wind-tunnel data by Westin *et al.* (1994), which are of utmost importance because they include distributions not only of the r.m.s. of the streamwise velocity fluctuations, but also of the fluctuating energy divided into bands centred at a single frequency. The Klebanoff modes were generated in a flat-plate laminar boundary layer by nearly isotropic free-stream turbulence evolving on a mean flow of $U_{\infty} = 8\,\mathrm{m\,s^{-1}}$. The boundary-layer thickness varied between about 5 and 7 mm at the measurement locations. As the wind-tunnel single-frequency data in figure 12(*a*) in Westin *et al.* (1994) were obtained from a decomposition of a full spectrum of turbulence, while our calculations correspond to the evolution of a single Fourier mode, a few assumptions are necessary to carry out the comparison:

(*a*) Small-amplitude fluctuations. We assume that the boundary-layer fluctuations can be treated as linearized perturbations about the Blasius flow. This is reasonable at $x^* = 500$ mm because the mean flow measurements shown in figure 6 in Westin *et al.* (1994, p. 205) deviate only about 1% or less from the laminar solution. This hypothesis

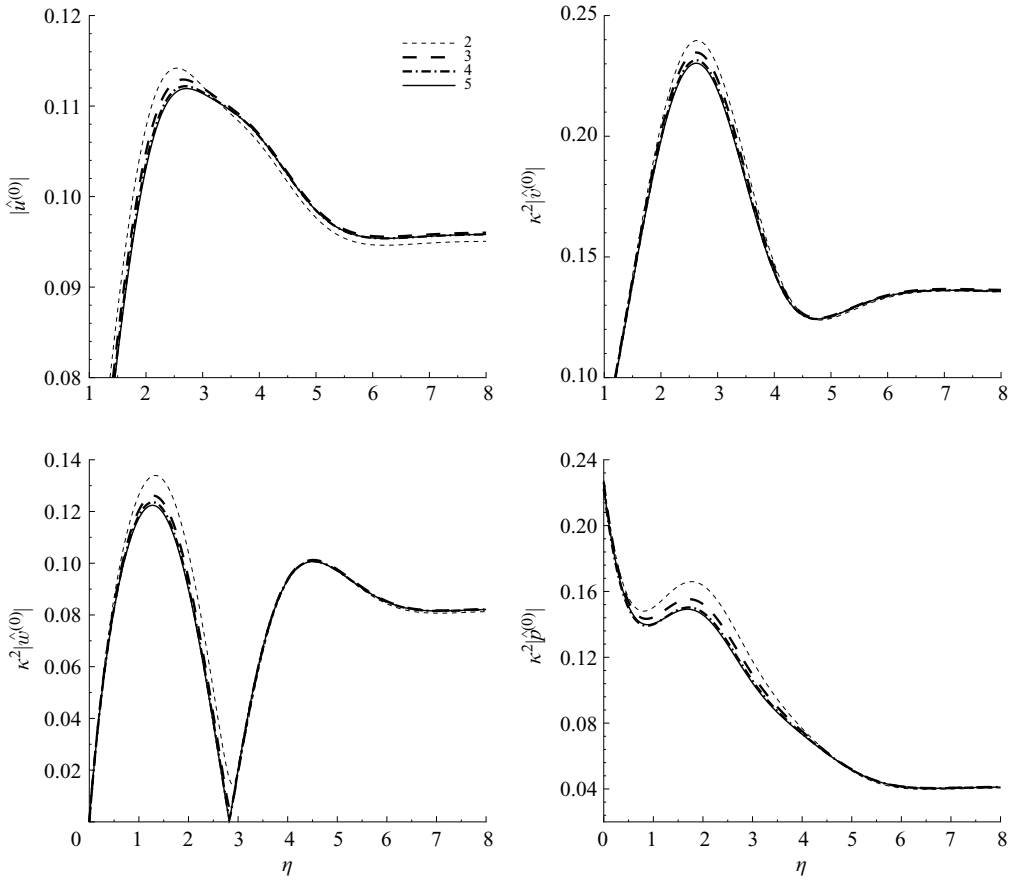

FIGURE 11. Asymptotic scaling of boundary-region quantities for $\kappa \to \infty$, $\kappa_2/\kappa = 1$ at $\kappa^2\overline{x} = 1$. The numbers in the legend indicate κ.

is arguably not applicable at the farthest measurement point ($x^* = 1000$ mm), which is near the transition location. Under this assumption, it follows that each vortical structure corresponding to a Fourier mode may be assumed to evolve independently, and the gust-convection relation $k_x^* = \omega^*/U_\infty$ holds. The streamwise wavelength λ_x^* and the $\overline{x}$ position can be estimated. The assumption of small amplitude also implies that the spanwise wavelength remains constant as the flow evolves downstream, which is consistent with the observations of Westin *et al.* (1994).

(*b*) Axisymmetric turbulence in y–z plane. We assume that the free-stream turbulence is axisymmetric, i.e. homogeneous and isotropic in y–z planes perpendicular to the mean flow (Batchelor 1946; Chandrasekhar 1950). The measurements show that the statistics of the fluctuating velocity components along these directions assume almost the same values and are uniforms in such planes. The r.m.s. of the streamwise velocity component is instead three–four times larger. The integral and Taylor length scales along the y and z directions are comparable, while they are two–three times larger along the streamwise direction. Therefore, it appears legitimate to assume that $\lambda_y^*=\lambda_z^*$ (i.e. $\kappa_2=\kappa$) and $\hat{u}_2^\infty=\hat{u}_3^\infty$. We set $\hat{u}_1^\infty = 1$ without losing generality because the data will be rescaled by the maximum of the squared streamwise velocity of the corresponding experimental profile.

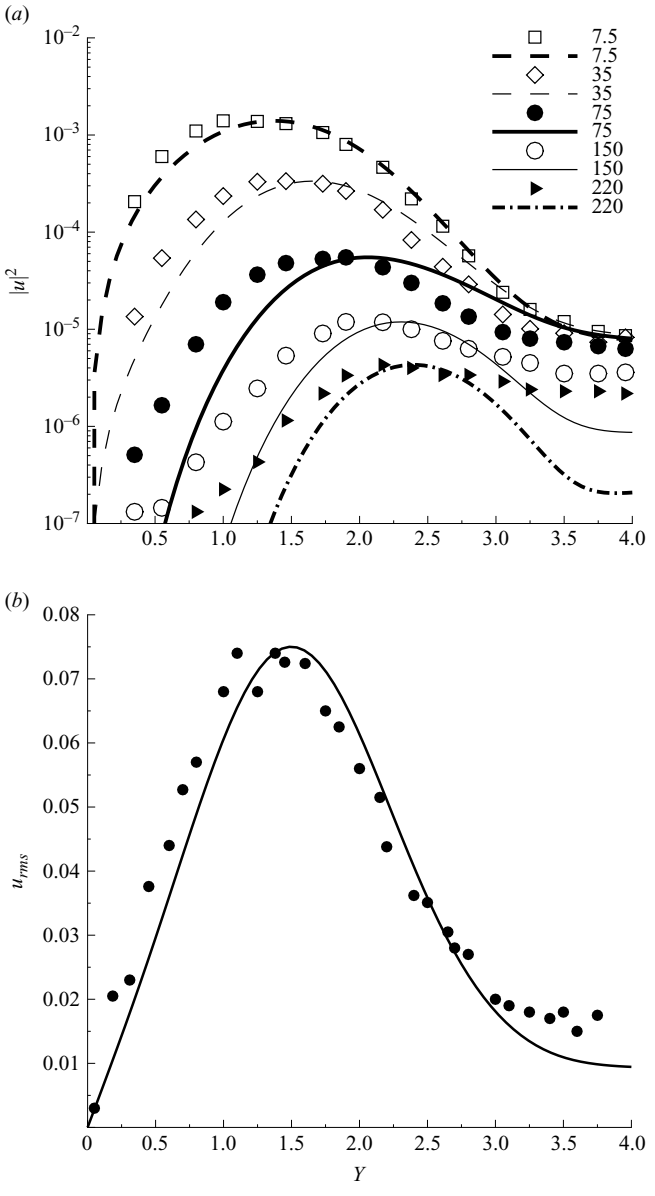

FIGURE 12. Profiles of (*a*) fluctuating energy for different frequencies $\hat{F}=10^6 f$ and (*b*) u_{rms} as functions of $Y = y^*/\delta_d^*$. Lines denote the numerical calculations and symbols the experimental data by Westin *et al.* (1994) at $x^* = 500\,\mathrm{mm}$ for $U_\infty = 8\,\mathrm{m\,s^{-1}}$.

In order to fully specify the problem, we must estimate the spanwise wavelength λ_z^* and $\hat{u}_3^\infty$. As no information is provided on how these quantities vary with the frequency for each Fourier component, we resort to the numerical calculations. Following the result shown in figure 2 in Leib *et al.* (1999, p. 178), i.e. at leading order the position of the maximum only depends on κ (and therefore on λ_z^* for given U_∞, ν, λ_x^*), we estimate $\lambda_z^* = \lambda_z^*(\kappa)$ through our numerical database by determining κ for which the maximum of the Klebanoff modes given in figure 12(*a*) in Westin *et al.* (1994) agrees with the numerical η_{max}. The velocity component $\hat{u}_3^\infty$ is estimated in similar fashion through

$\hat{F}$	k_1	f^*(Hz)	λ_x^* (mm)	λ_z^* (mm)	κ	$\overline{x}$
7.5	0.034	5.12	1560	8.5	0.50	2.01
35	0.123	23.91	335	6.6	0.30	9.39
75	0.272	51.24	156	6.8	0.20	20.12
150	0.378	102.49	78	4.7	0.20	40.25
220	0.518	150.32	53	4.4	0.17	59.03

TABLE 1. Estimated flow quantities of experimental data shown in figure 12(*a*) in Westin *et al.* (1994, p. 210).

the comparison of the ratio between the experimental $|u|_{max}$ and $|u|$ in the free stream with $C/(k_1 C^{(0)}) \approx \sqrt{2}\hat{u}_3^{\infty}/(k_1\hat{u}_1^{\infty})$. The latter is a reasonable approximation of the ratio of the experimental quantities because the dominant part in the first equation of (2.8) peaks in the core of the boundary layer, while the lower-order component is likely to reach its maximum in the free stream. Table 1 gives our estimates for the experimental conditions of the data of Westin *et al.* (1994) in figure 12(*a*). As expected, $\kappa = O(1)$ or smaller, and the estimated values for λ_z^* are comparable with the streak spacing $\sim$7 mm measured by Westin *et al.* (1994). It is also found that $\lambda_x^* \gg \lambda_z^*, \delta^*$, as required by the asymptotic analysis.

Figure 12(*a*) presents the comparison between the profiles of the fluctuating energy and our calculations of the full Klebanoff mode solution $\overline{u}_0$ in (2.8), rescaled by the maxima of each experimental profile. The overall agreement is good, especially for the low-frequency fluctuations. The low-frequency fluctuations penetrate more deeply into the boundary layer and are amplified more than the high-frequency fluctuations. These are located in the proximity of the free stream, as predicted by the theory of the edge-layer confinement (Gulyaev *et al.* 1989; Leib *et al.* 1999). The better agreement for data at low frequency may be due to the higher uncertainty for high-frequency fluctuations, which are of smaller amplitude. Another source of error could be that the calculation are carried out at a specified frequency $\hat{F}$, while it is not clear how wide the frequency band centred at $\hat{F}$ actually is for the profiles in figure 12(*a*). In figure 12(*b*), a good agreement between our calculations and the u_{rms} profile by Westin *et al.* (1994) in figure 9(*b*) is shown. As no detailed information is provided about the free-stream spectrum, we have computed the numerical trend by summing the profiles in figure 12(*a*). Note that the rescaling by the maximum of the experimental u_{rms} is performed after the summation.

4.2. *Boundary-layer receptivity by free-stream vortical disturbances interacting with localized wall inhomogeneities*

The receptivity of the Blasius boundary layer to a two-dimensional gust interacting with localized wall perturbations is studied in this section. We investigate how the absolute value of the efficiency function Λ_u of the streamwise velocity component varies as a function of the frequency f of the gust at a downstream Reynolds number $Re_\delta = 1216.78$ ($Re_x = 5 \times 10^5$, as in figures 5 and 6 in Choudhari 1996). At this Re_δ, there exists a wide range of frequencies f for which the eigenmodes are unstable, as shown by the growth rates in figure 13 (dashed line). Although the physical location x^* of the wall perturbation is constant since Re_δ is unvaried, the scaled streamwise distance $\overline{x}$ used for the LUBR computations grows with f (see (2.31)). The location $\overline{x}$ changes from 5 to about 50 in the range of frequency considered. It is first checked that approximation (2.33) for the gust response holds in the unstable range of frequencies.

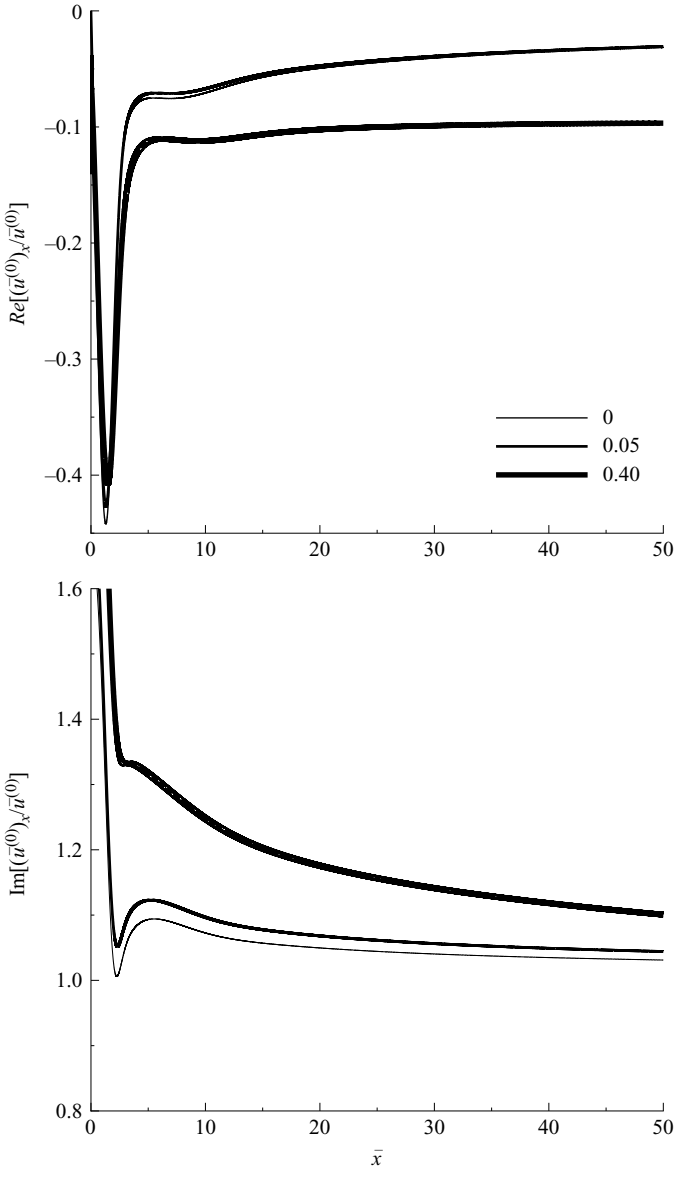

FIGURE 13. Scaled wall-normal wavenumber κ_2 as a function of f at $Re_\delta = 1216.78$. The values in the legend indicate $\hat{u}_2^\infty$. The line with symbols indicates the growth rate of the TS wave, $-20 \times \mathrm{Im}(\alpha_{TS})$. The $\hat{u}_2^\infty = -1.0$ line is not shown because $\kappa_2 = 0$.

Figure 14 shows that the real and imaginary parts of the ratio $(\overline{u}^{(0)})_{\bar{x}}/\overline{u}^{(0)}$ (where the subscript indicates partial differentiation with respect of $\bar{x}$) are largely independent of $\bar{x}$ in the $\bar{x}$ range in which the TS waves are unstable, $20 < \bar{x} < 50$. This shows that the gust has an exponential-like behaviour where the TS waves are unstable. It is also evident that such an approximation is not valid for smaller $\bar{x} = O(1)$, which confirms that the Orr–Sommerfeld and Squire equations, in which the streak behaviour is treated as wave-like, cannot be employed to study the laminar streaks because the non-parallel effects are relevant there and cannot be ignored.

The corresponding values of κ_2 are displayed in figure 13 ($\kappa = 0$ because the forcing gust is two-dimensional). Each curve corresponds to a different wall-normal velocity

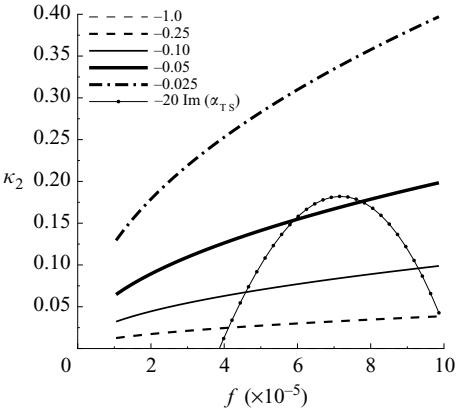

FIGURE 14. Real and imaginary parts of the ratio $(\overline{u}^{(0)})_x/\overline{u}^{(0)}$ at $\eta = 2$ as a function of $\overline{x}$. The numbers in the legend indicate κ_2.

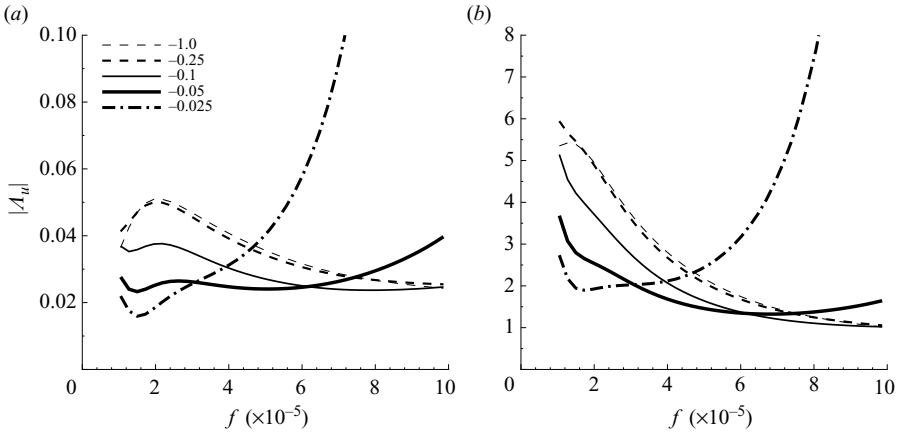

FIGURE 15. Amplitude of Λ_u versus f (a) for wall roughness and (b) wall suction. The values in the legend indicate $\hat{u}_2^{\infty}$.

component of the gust, $\hat{u}_2^{\infty}$, or to a different $\theta_g = \arccos(\hat{u}_2^{\infty})$. For a fixed frequency, from the definition of κ_2 given in the 'Introduction', (2.1) and (2.2), it follows that κ_2 grows as $\hat{u}_2^{\infty}$ decreases in amplitude (and $\theta_g \to \pi/2$). The effects of a small wall-normal wavelength are therefore expected to intensify as $\hat{u}_2^{\infty}$ decreases, i.e. for gusts mainly oriented along the streamwise direction. Note that when $\kappa_2 = O(1)$, the numerical computation of Λ_u takes a much longer time than when $\kappa_2 = 0$. Indeed, as f and κ_2 vary, each Λ_u computation requires that the integration of the LUBR equations be started from the proximity of the leading edge, whereas when $\kappa_2 = 0$, the correct vorticity signature can be obtained by integration from the $\overline{x}$ position corresponding to the previous f.

Figure 15 shows $|\Lambda_u|$ as a function of f (a) for the wall-roughness case and (b) for the wall-suction case. The profiles are qualitatively similar in the two cases, but the wall-suction values are about two order of magnitudes larger. The efficiency function first decreases as θ_g grows, but eventually the effect of a small wall-normal wavelength is to amplify $|\Lambda_u|$ significantly when $\kappa_2 = O(1)$. This growth is mainly caused by the shape of the streamwise disturbance velocity profile. For small wall-normal wavelengths, figures 4 and 6(a) show that the amplitude of the streamwise fluctuations decreases more rapidly in the free stream than within the boundary layer

because the shear of the mean flow works as an amplifier and counteracts the viscous dissipation effects, a phenomenon which is more intense as κ_2 grows. The shape of the streamwise velocity profile is therefore significantly different from the boundary-layer case, $\kappa_2 = 0$ and $\hat{u}_2^{\infty} = \pm 1.0$, where, for this range of $\bar{x}$ locations, the streamwise velocity disturbance within the boundary layer is always lower than in the free stream (see figure 2 in Choudhari 1996, p. 10). For the receptivity calculations, the velocity disturbances are rescaled by the amplitude of the free-stream streamwise component, so that the peak of streamwise velocity becomes responsible for an intense nonlinear forcing that amplifies $|\Lambda_u|$. Indeed, the forcing amplitude has been found to grow with $\bar{x}$ and κ_2.

We close this section by pointing out some differences between the present vorticity-induced receptivity and the analogous acoustic receptivity. Firstly, in the vorticity case, the nonlinear terms are concentrated in the core of the boundary layer, while in the latter case the induced perturbation is much closer to the wall (see figure 7 in Choudhari & Streett 1992, p. 2505). The relative contribution of the inhomogeneous wall boundary conditions and of the nonlinear forcing terms on the efficiency function is also of interest. The influence of the boundary conditions has been found to be negligible in the vorticity case by setting the wall boundary condition to zero in (2.35) and by retaining the nonlinear terms in (2.34) (a technique also used by Choudhari & Streett 1992). The main reason for this is that the vorticity response is not confined to the proximity of the wall, so that the wall-shear stress of the streamwise perturbation, U_{gY}, appearing in the wall boundary conditions (2.35), is small, and its influence on the TS-wave scattering is limited. This scenario is in marked contrast with the receptivity to acoustic forcing, where the nonlinear terms and the wall boundary condition have a comparable (and partly mutually cancelling) effect (Choudhari & Streett 1992).

5. Summary

There has recently been considerable interest in the theoretical modelling of the laminar streaks (or Klebanoff modes), namely the streamwise-elongated, low-frequency disturbances appearing in pre-transitional laminar boundary layers as a consequence of a medium-to-high level of free-stream turbulence. The reason for this lies in the belief that the streaks may be responsible for the so-called bypass transition, namely the breakdown to turbulence via some mechanism which is alternative to the slower, classical instability route involving TS waves propagating in a purely laminar boundary layer. Experimental evidence indeed shows that when the free stream is sufficiently disturbed by vortical fluctuations, the laminar streaks quickly evolve into turbulence spots.

A mathematical framework for the laminar streaks which can be regarded as all-inclusive is the one by Leib *et al.* (1999). Their asymptotic analysis in the limit of small-amplitude and low-frequency disturbances shows that relevant features such as the streak unsteadiness, the non-parallel effects, the spanwise viscous diffusion and the influence of free-stream fluctuations are all of the same order of magnitude and are therefore taken into account.

In the present work, the study of Leib *et al.* (1999) has been extended to compute (i) the boundary-layer vorticity signature induced by a two-dimensional free-stream gust with a small wall-normal wavelength, (ii) the second-order terms of a fully three-dimensional Klebanoff mode and (iii) the TS wave excited when a two-dimensional vorticity fluctuation such as the one in (i) interacts nonlinearly with a small localized wall perturbation.

The interest in (i) resides in the fact that Leib *et al.* (1999) did study the response of a three-dimensional gust with wall-normal and spanwise wavelengths comparable with the boundary-layer thickness and also that of only a two-dimensional gust with wall-normal wavelength which is asymptotically larger than the boundary-layer thickness. The first part of the present study has therefore focused on the effect of the two-dimensional-gust viscous dissipation and wall-normal displacement on the boundary-layer signature, namely on the influence of wall-normal wavelengths which are comparable with the layer thickness. In this case, it is found that the streamwise velocity profile shows a marked peak in the core of the boundary layer and that the wall-normal velocity profile presents a wavy character as the free stream is approached.

We have carried out part (ii) of the analysis because the second-order terms of the vorticity signature, which are negligible in the core of the boundary layer, may become dominant in the outer portion of the boundary layer. The profiles of the Klebanoff modes have been compared with the distributions of fluctuating energy at different frequencies measured by Westin *et al.* (1994). A good agreement has been attained by assuming that the perturbations are of small amplitude and axisymmetric in planes perpendicular to the mean flow. Our estimates have also successfully reproduced the r.m.s. of the streamwise velocity fluctuations.

The effect of small-wavelength gusts on the scattering of TS waves (iii) has been found to be significant because of the difference in magnitude of the streamwise velocity in the core of the boundary layer and in the outer portion near the free stream. This part of the analysis could be viewed as a contribution to the long-standing effort to understand the interplay between the Klebanoff modes and the TS waves. Future work should be directed to more complex scenarios, such as the receptivity of three-dimensional gusts interacting with three-dimensional, distributed wall inhomogeneities.

It is our hope that the present analysis will motivate further experimental investigation. For example the accurate study by Dietz (1999) may be extended to generate two-dimensional free-stream gusts with wall-normal wavelengths comparable with the boundary-layer thickness, so that the present theoretical analysis may be validated. The gust may still be produced by a thin vibrating ribbon, and the small wall-normal wavelength could be fixed by the inclination of the plane of oscillation with respect to the direction of the free-stream mean flow. An even more involved experiment would focus on the boundary-layer response to a single three-dimensional Klebanoff mode, which would allow a detail comparison with our results and those of Leib *et al.* (1999). As opposed to a straight ribbon as in the work of Dietz (1999), a wavy, vibrating (or rotating) thin ribbon could be used, thereby allowing the precise specification of the gust amplitude and frequency and its wall-normal and spanwise wavelengths. Bypass transition induced by a combination of medium-to-high free-stream turbulence and distributed roughness would also be of great practical interest.

I acknowledge the help of Professor Tapan K. Sengupta and Professor Thomas Bridges on the compound matrix method for the solution of the Orr–Sommerfeld equation. I would like to thank the referees for their useful suggestions and Dr M. E. Goldstein for his insightful comments on a preliminary version of the paper.

Appendix A. Power series equations for initial conditions

The equations for the power series terms in (2.30) and their boundary conditions are presented. Differently from Leib *et al.* (1999), the wall-normal and spanwise components are now singular as $\bar{x} \to 0^+$. The first three terms are retained in order to

start the marching procedure correctly. Note that for $\{\overline{u}, \overline{v}, \overline{w}, \overline{p}\}$ only two terms are sufficient. The third terms are now necessary to make the components $\overline{v}^{(0)}, \overline{w}^{(0)}$ satisfy the no-slip condition at the wall as $\overline{x} \to 0^+$. By substituting (2.30) into the LUBR equations (2.9)–(2.12) and by collecting like powers of $\overline{x}$, three systems of ordinary differential equations are obtained:

$$V_0' - \eta U_0' = 0, \tag{A1}$$

$$\eta F'' U_0 + F U_0' + U_0'' - F'' V_0 = 0, \tag{A2}$$

$$P_0' = 0, \tag{A3}$$

$$F' W_0 + F W_0' + W_0'' + \kappa^2 P_0 = 0, \tag{A4}$$

$$U_1 - \eta U_1' + V_1' + W_0 = 0, \tag{A5}$$

$$(F' - \eta F'') U_1 - F U_1' - U_1'' + F'' V_1 = 0, \tag{A6}$$

$$P_1' = (2F' - (\eta F')') V_0 + F V_0' + V_0'' + (\eta(\eta F')' - F) U_0, \tag{A7}$$

$$F W_1' + W_1'' + \kappa^2 P_1 = 0, \tag{A8}$$

$$2U_2 - \eta U_2' + V_2' + W_1 = 0, \tag{A9}$$

$$(2F' - \eta F'') U_2 - F U_2' - U_2'' + F'' V_2 + (\kappa^2 - \mathrm{i}) U_0 = 0, \tag{A10}$$

$$P_2' = (F' - (\eta F')') V_1 + F V_1' + V_1'' + (\eta(\eta F')' - F) U_1, \tag{A11}$$

$$F' W_2 - F W_2' - W_2'' - \kappa^2 P_2 + (\kappa^2 - \mathrm{i}) W_0 = 0. \tag{A12}$$

The velocity components in (A1)–(A12) satisfy the no-slip condition at the wall. The outer boundary conditions are found as follows. Firstly, the power series expansion for $\overline{u}^{(0)}$ is matched with the $\overline{x} \ll 1$ expansion of its large-η solution (2.13) to obtain

$$U_0 \to 1, \;\; U_1 \to \mathrm{i}(\kappa_2 + \mathrm{i}|\kappa|)\overline{\eta},$$
$$U_2 \to (1/2)\left(\mathrm{i} - \kappa_2(\kappa_2 + \mathrm{i}|\kappa|) - \frac{\kappa_2^3 + \mathrm{i}|\kappa|^3}{\kappa_2 - \mathrm{i}|\kappa|}\overline{\eta}^2\right) \quad \text{as } \eta \to \infty.$$

The $\overline{x} \ll 1$ expansion of the large-η solution (2.15) for $\overline{w}^{(0)}$ is matched with the leading-order term in the power series expansion to find

$$W_0 \to -\frac{\beta|\kappa|(\kappa_2 - \mathrm{i}|\kappa|)}{2(\kappa_2 + \mathrm{i}|\kappa|)}, \text{ as } \eta \to \infty, \text{ and } P_0 = \frac{\beta(\kappa_2 - \mathrm{i}|\kappa|)}{2|\kappa|(\kappa_2 + \mathrm{i}|\kappa|)}.$$

The large-η wall-normal velocity component (2.14) is matched at leading order with the initial condition for the boundary-layer equations, given by (4.13) in Leib *et al.* (1999), namely $\overline{v}^{(0)} \to \beta/(4\overline{x})$. It is found that

$$\int_0^{\overline{x}} g^{(0)}(\check{x}) \mathrm{e}^{-\mathrm{i}\check{x}} \mathrm{d}\check{x} = \frac{\beta}{|\kappa|(2\overline{x})^{1/2}}\left(1 - \frac{\kappa_2\left(3\kappa_2^2 - \kappa\right)}{2(\kappa_2 - \mathrm{i}|\kappa|)\left(\kappa^2 + \kappa_2^2\right)}\right) + \frac{g_1^{(0)}}{|\kappa|} + \frac{g_2^{(0)}(2\overline{x})^{1/2}}{|\kappa|} \ldots. \tag{A13}$$

The constants $g_1^{(0)}$, $g_2^{(0)}$ are found by matching the second-order term and the third-order term of the $\overline{x} \ll 1$ expansion of the large-η solution (2.14) for $\overline{v}^{(0)}$ as $\eta \to \infty$ with the numerical solution for V_1 and V_2, respectively. It follows that

$$g_1^{(0)} = V_{1,0} + \mathrm{i}(\kappa_2 + \mathrm{i}|\kappa|) + \beta^2\left(-3|\kappa|/2 + \frac{|\kappa|\kappa_2}{2(\kappa_2 - \mathrm{i}\kappa)} + \frac{\kappa_2}{(\kappa_2 - \mathrm{i}|\kappa|)\left(\kappa^2 + \kappa_2^2\right)}\right.$$
$$\left. \times \left(|\kappa|\left(3\kappa_2^2 - \kappa^2\right)/2 + \mathrm{i}\kappa_2\left(\kappa_2^2 - \kappa^2\right)\right)\right),$$

where

$$V_{1,0} = \lim_{\eta\to\infty}\left(V_1 + \left(3|\kappa|\beta/2 - \frac{\mathrm{i}\kappa_2^2\beta}{\kappa_2 + \mathrm{i}|\kappa|}\right)\eta\right),$$

and

$$\begin{aligned} g_2^{(0)} = V_{2,0} &+ \frac{\beta}{4(\kappa_2 - \mathrm{i}|\kappa|)}\left(2\kappa_2\left(\kappa_2^2 - \kappa^2\right) + 8\mathrm{i}|\kappa|^3 + |\kappa|\right) \\ &- \frac{\mathrm{i}\beta(\kappa_2 - 2\mathrm{i}|\kappa|)}{4(\kappa_2 - \mathrm{i}|\kappa|)} - \beta\left(\mathrm{i} + |\kappa|g_1^{(0)}\right) + \beta\kappa_2(\kappa_2 + \mathrm{i}|\kappa|) \\ &+ \frac{\beta^3}{4(\kappa_2 - \mathrm{i}|\kappa|)}\left(3\mathrm{i}|\kappa|^3 + \frac{2\kappa_2^5 + 2\mathrm{i}|\kappa|^5 - 3\kappa^4\kappa_2 + 2\mathrm{i}|\kappa|^3\kappa_2^2 - \kappa^2\kappa_2^3}{\kappa^2 + \kappa_2^2}\right), \end{aligned}$$

where

$$V_{2,0} = \lim_{\eta\to\infty}(V_2 - V_{2,1}\eta - V_{2,2}\eta^2),\ V_{2,1} = \kappa_2(\kappa_2 + \mathrm{i}|\kappa|) - \mathrm{i} - |\kappa|g_1^{(0)} - 2\beta V_{2,2},$$

$$V_{2,2} = -\frac{\beta}{4(\kappa_2 - \mathrm{i}|\kappa|)}\left(3\mathrm{i}|\kappa|^3 + \frac{2\kappa_2^5 + 2\mathrm{i}|\kappa|^5 - 3\kappa^4\kappa_2 + 2\mathrm{i}|\kappa|^3\kappa_2^2 - \kappa^2\kappa_2^3}{\kappa^2 + \kappa_2^2}\right).$$

The $\overline{x} \ll 1$ expansion of the large-η solution (2.15) for $\overline{w}^{(0)}$ is matched with the second-order term in the power series expansion to find

$$\begin{aligned} W_1 &\to |\kappa|g_1^{(0)} - 3\kappa^2\beta\overline{\eta}/2, \\ W_2 &\to |\kappa|g_2^{(0)} - \kappa^2 g_1^{(0)}\overline{\eta} + \frac{\mathrm{i}\beta\kappa^2\left(\mathrm{i} - 4\kappa_2^2 - 8\kappa^2\right)}{4(\kappa_2 - \mathrm{i}|\kappa|)} + \frac{\beta|\kappa|\left(2|\kappa|^3 - \mathrm{i}\kappa_2^3 - 2|\kappa|\kappa_2^2 + 3\mathrm{i}\kappa_2\kappa^2\right)}{4(\kappa_2 - \mathrm{i}|\kappa|)\left(\kappa^2 + \kappa_2^2\right)} \\ &\quad - \frac{\beta\kappa^2\overline{\eta}^2\left(5\mathrm{i}\kappa^4 - 3|\kappa|^3\kappa_2 + 5\mathrm{i}\kappa^2\kappa_2^2 + |\kappa|\kappa_2^3 + 4\mathrm{i}\kappa_2^4\right)}{4(\kappa_2 - \mathrm{i}|\kappa|)\left(\kappa^2 + \kappa_2^2\right)} \quad \text{as } \eta \to \infty \end{aligned}$$

and

$$\begin{aligned} P_1 &\to 3\beta\overline{\eta}/2, \\ P_2 &\to g_2^{(0)}|\kappa| + \frac{\mathrm{i}\beta\kappa_2^3}{4|\kappa|(\kappa_2 - \mathrm{i}|\kappa|)\left(\kappa^2 + \kappa_2^2\right)} + \frac{\beta\left(-\kappa^2 + 3\kappa_2^2 - 3\mathrm{i}|\kappa|\kappa_2 + 4\mathrm{i}\kappa^2\kappa_2^2 + 4\mathrm{i}\kappa_2^4\right)}{4(\kappa_2 - \mathrm{i}|\kappa|)\left(\kappa^2 + \kappa_2^2\right)} \\ &\quad + \frac{\beta\overline{\eta}^2\left(5\mathrm{i}\kappa^4 - 3|\kappa|^3\kappa_2 + 5\mathrm{i}\kappa^2\kappa_2^2 + |\kappa|\kappa_2^3 + 4\mathrm{i}\kappa_2^4\right)}{4(\kappa_2 - \mathrm{i}|\kappa|)\left(\kappa^2 + \kappa_2^2\right)} \quad \text{as } \eta \to \infty. \end{aligned}$$

Appendix B. Initial conditions for the boundary-region equations

The initial conditions to be imposed for $\{\overline{u}^{(0)}, \overline{v}^{(0)}, \overline{w}^{(0)}, \overline{p}^{(0)}\}$ at $\overline{x} \ll 1$ are

$$\begin{aligned} \overline{u}^{(0)} \to U_0 + (2\overline{x})^{1/2}U_1 + 2\overline{x}U_2 &+ \frac{\mathrm{e}^{\mathrm{i}\overline{x}}}{\kappa_2 - \mathrm{i}|\kappa|}\left(\kappa_2\mathrm{e}^{\mathrm{i}\kappa_2(2\overline{x})^{1/2}\overline{\eta} - (\kappa^2 + \kappa_2^2)\overline{x}} - \mathrm{i}|\kappa|\mathrm{e}^{-|\kappa|(2\overline{x})^{1/2}\overline{\eta}}\right) \\ &- 1 - \mathrm{i}(2\overline{x})^{1/2}(\kappa_2 + \mathrm{i}|\kappa|)\overline{\eta} + \left(-\mathrm{i} + \kappa_2(\kappa_2 + \mathrm{i}|\kappa|) + \frac{\kappa_2^3 + \mathrm{i}|\kappa|^3}{\kappa_2 - \mathrm{i}|\kappa|}\overline{\eta}^2\right)\overline{x}, \end{aligned} \tag{B1}$$

$$\overline{v}^{(0)} \to \frac{V_0}{2\overline{x}} + \frac{V_1}{(2\overline{x})^{1/2}} + V_2 + \frac{\mathrm{e}^{\mathrm{i}\overline{x}-|\kappa|(2\overline{x})^{1/2}\overline{\eta}}}{(\kappa_2-\mathrm{i}|\kappa|)(2\overline{x})^{1/2}}\Bigg(-2\mathrm{i}|\kappa|^3\beta(2\overline{x})^{1/2} + 1 + \mathrm{i}\kappa^2\beta\overline{\eta} + \frac{i|\kappa|\beta}{2(2\overline{x})^{1/2}}\Bigg) + \mathrm{e}^{\mathrm{i}\overline{x}-|\kappa|(2\overline{x})^{1/2}\overline{\eta}}\left(\frac{\beta}{2\overline{x}}\left(1-\frac{\kappa_2\left(3\kappa_2^2-\kappa^2\right)}{2(\kappa_2-\mathrm{i}|\kappa|)\left(\kappa^2+\kappa_2^2\right)}\right)+\frac{g_1^{(0)}}{(2\overline{x})^{1/2}}+g_2^{(0)}\right) + \frac{\mathrm{e}^{\mathrm{i}\overline{x}+\mathrm{i}\kappa_2(2\overline{x})^{1/2}\overline{\eta}-(\kappa^2+\kappa_2^2)\overline{x}}}{\kappa_2-\mathrm{i}|\kappa|}\left(\frac{\kappa_2\beta\left(\kappa_2^2-\kappa^2\right)}{2\overline{x}\left(\kappa^2+\kappa_2^2\right)}-\frac{1+\mathrm{i}\left(\kappa^2+\kappa_2^2\right)}{(2\overline{x})^{1/2}}\right)-\frac{\beta}{4\overline{x}} - \frac{1}{(2\overline{x})^{1/2}}\left(g_1^{(0)}-\mathrm{i}(\kappa_2+\mathrm{i}|\kappa|)+\frac{\beta\overline{\eta}\left(2\mathrm{i}\kappa_2^4+3\mathrm{i}\kappa^4+\mathrm{i}\kappa^2\kappa_2^2+|\kappa|\kappa_2^3-3|\kappa|^3\kappa_2\right)}{2(\kappa_2-\mathrm{i}|\kappa|)\left(\kappa^2+\kappa_2^2\right)}\right) - g_2^{(0)}+\frac{\beta}{4(\kappa_2-\mathrm{i}|\kappa|)}\left(2\kappa_2\left(\kappa_2^2-\kappa^2\right)+8\mathrm{i}|\kappa|^3+|\kappa|\right)-\frac{\mathrm{i}\beta(\kappa_2-2\mathrm{i}|\kappa|)}{4(\kappa_2-\mathrm{i}|\kappa|)}+\overline{\eta}\big(\mathrm{i}+|\kappa|g_1^{(0)} - \kappa_2(\kappa_2+\mathrm{i}|\kappa|)\big)+\frac{\beta\overline{\eta}^2}{4(\kappa_2-\mathrm{i}|\kappa|)}\left(3\mathrm{i}|\kappa|^3+\frac{2\kappa_2^5+2\mathrm{i}|\kappa|^5-3\kappa^4\kappa_2+2\mathrm{i}|\kappa|^3\kappa_2^2-\kappa^2\kappa_2^3}{\kappa^2+\kappa_2^2}\right), \tag{B2}$$

$$\overline{w}^{(0)} \to \frac{W_0}{(2\overline{x})^{1/2}} + W_1 + (2\overline{x})^{1/2}W_2 + |\kappa|\mathrm{e}^{\mathrm{i}\overline{x}-|\kappa|(2\overline{x})^{1/2}\overline{\eta}}\left(\frac{\beta}{(2\overline{x})^{1/2}}\left(1-\frac{\kappa_2\left(3\kappa_2^2-\kappa^2\right)}{2(\kappa_2-\mathrm{i}|\kappa|)\left(\kappa^2+\kappa_2^2\right)}\right) + g_1^{(0)}+g_2^{(0)}(2\overline{x})^{1/2}\right)+\frac{\mathrm{i}\beta\kappa^2\mathrm{e}^{\mathrm{i}\overline{x}-|\kappa|(2\overline{x})^{1/2}\overline{\eta}}}{(\kappa_2-\mathrm{i}|\kappa|)(2\overline{x})^{1/2}}(1/2+|\kappa|\left(2\overline{x}\right)^{1/2}\overline{\eta}) + \frac{2\mathrm{i}\beta\kappa^2\kappa_2^2\ \mathrm{e}^{\mathrm{i}\overline{x}+\mathrm{i}\kappa_2(2\overline{x})^{1/2}\overline{\eta}-(\kappa^2+\kappa_2^2)\overline{x}}}{(2\overline{x})^{1/2}(\kappa_2-\mathrm{i}|\kappa|)\left(\kappa^2+\kappa_2^2\right)}+\frac{\beta|\kappa|(\kappa_2-\mathrm{i}|\kappa|)}{2(2\overline{x})^{1/2}(\kappa_2+\mathrm{i}|\kappa|)}-g_1^{(0)}|\kappa|+(3/2)\kappa^2\beta\overline{\eta}-(2\overline{x})^{1/2} \times\left(|\kappa|g_2^{(0)}-\kappa^2g_1^{(0)}\overline{\eta}+\frac{\mathrm{i}\beta\kappa^2\left(\mathrm{i}-4\kappa_2^2-8\kappa^2\right)}{4(\kappa_2-\mathrm{i}|\kappa|)}+\frac{\beta|\kappa|\left(2|\kappa|^3-\mathrm{i}\kappa_2^3-2|\kappa|\kappa_2^2+3\mathrm{i}\kappa_2\kappa^2\right)}{4(\kappa_2-\mathrm{i}|\kappa|)\left(\kappa^2+\kappa_2^2\right)} - \frac{\beta\kappa^2\overline{\eta}^2\left(5\mathrm{i}\kappa^4-3|\kappa|^3\kappa_2+5\mathrm{i}\kappa^2\kappa_2^2+|\kappa|\kappa_2^3+4\mathrm{i}\kappa_2^4\right)}{4(\kappa_2-\mathrm{i}|\kappa|)\left(\kappa^2+\kappa_2^2\right)}\right), \tag{B3}$$

$$\overline{p}^{(0)} \to \frac{P_0}{(2\overline{x})^{3/2}} + \frac{P_1}{2\overline{x}} + \frac{P_2}{(2\overline{x})^{1/2}} - \frac{\beta\mathrm{e}^{\mathrm{i}\overline{x}-|\kappa|(2\overline{x})^{1/2}\overline{\eta}}}{|\kappa|\,(2\overline{x})^{3/2}}\left(1-\frac{\kappa_2\left(3\kappa_2^2-\kappa^2\right)}{2\left(\kappa_2-\mathrm{i}|\kappa|\right)\left(\kappa^2+\kappa_2^2\right)}\right) + \frac{g_2^{(0)}\mathrm{e}^{\mathrm{i}\overline{x}-|\kappa|(2\overline{x})^{1/2}\overline{\eta}}}{|\kappa|(2\overline{x})^{1/2}} - \frac{\mathrm{i}\beta\mathrm{e}^{\mathrm{i}\overline{x}-|\kappa|(2\overline{x})^{1/2}\overline{\eta}}}{2|\kappa|\,(2\overline{x})^{1/2}}\left(1-\frac{\kappa_2\left(3\kappa_2^2-\kappa^2\right)}{2\left(\kappa_2-\mathrm{i}|\kappa|\right)\left(\kappa^2+\kappa_2^2\right)}\right) - \frac{\mathrm{i}\beta\mathrm{e}^{\mathrm{i}\overline{x}}}{(2\overline{x})^{3/2}(\kappa_2-\mathrm{i}|\kappa|)}\left(\left(1/2+|\kappa|(2\overline{x})^{1/2}\overline{\eta}\right)\mathrm{e}^{-|\kappa|(2\overline{x})^{1/2}\overline{\eta}}+\frac{2\kappa_2^2\ \mathrm{e}^{\mathrm{i}\kappa_2(2\overline{x})^{1/2}\overline{\eta}-(\kappa^2+\kappa_2^2)\overline{x}}}{\kappa^2+\kappa_2^2}\right) - \frac{\beta(\kappa_2-\mathrm{i}|\kappa|)}{2(2\overline{x})^{3/2}|\kappa|(\kappa_2+\mathrm{i}|\kappa|)}-\frac{3\beta\overline{\eta}}{4\overline{x}}-\frac{1}{(2\overline{x})^{1/2}}\left(g_2^{(0)}/|\kappa|+\frac{\mathrm{i}\beta\kappa_2^3}{4|\kappa|\left(\kappa_2-\mathrm{i}|\kappa|\right)\left(\kappa^2+\kappa_2^2\right)} + \frac{\beta\left(-\kappa^2+3\kappa_2^2-3\mathrm{i}|\kappa|\kappa_2+4\mathrm{i}\kappa^2\kappa_2^2+4\mathrm{i}\kappa_2^4\right)}{4(\kappa_2-\mathrm{i}|\kappa|)\left(\kappa^2+\kappa_2^2\right)} + \frac{\beta\overline{\eta}^2\left(5\mathrm{i}\kappa^4-3|\kappa|^3\kappa_2+5\mathrm{i}\kappa^2\kappa_2^2+|\kappa|\kappa_2^3+4\mathrm{i}\kappa_2^4\right)}{4(\kappa_2-\mathrm{i}|\kappa|)\left(\kappa^2+\kappa_2^2\right)}\right). \tag{B4}$$

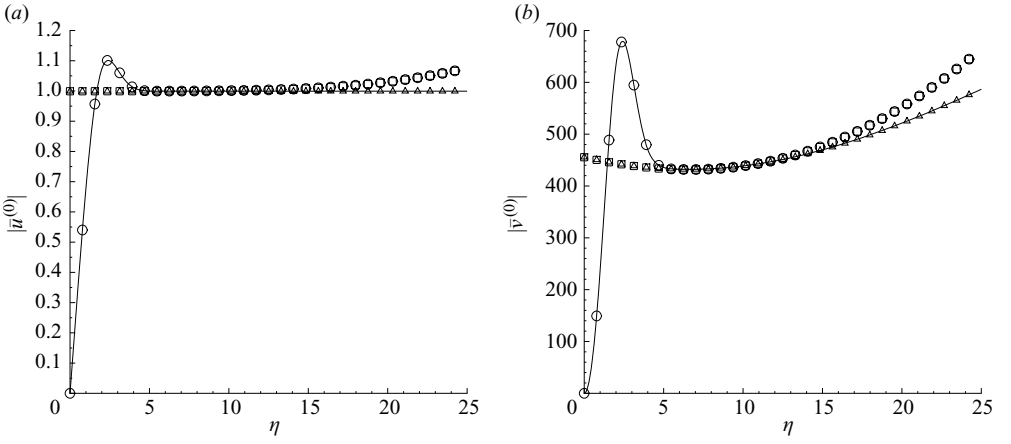

FIGURE 16. Amplitude of (a) streamwise $\overline{u}^{(0)}$ and (b) wall-normal $\overline{v}^{(0)}$ velocity profiles for $\kappa = 0$ and $\kappa_2 = 1$ at $\overline{x} = 7 \times 10^{-4}$ obtained by the initial composite solutions (B1) and (B2). The symbols are as follows: ○, inner solution; △, outer solution; □, common part; solid line, composite solution.

For a two-dimensional gust, the initial conditions reduce to

$$\overline{u}^{(0)} \to U_0 + (2\overline{x})^{1/2} U_1 + 2\overline{x} U_2 + \mathrm{e}^{\mathrm{i}\overline{x} + \mathrm{i}\kappa_2 (2\overline{x})^{1/2}\overline{\eta} - \kappa_2^2 \overline{x}} - 1 - \mathrm{i}\overline{\eta}\kappa_2 (2\overline{x})^{1/2} + \left(-\mathrm{i} + \kappa_2^2 \left(1 + \overline{\eta}^2\right)\right) \overline{x}, \quad \text{(B5)}$$

$$\begin{aligned} \overline{v}^{(0)} \to {} & \frac{V_0}{2\overline{x}} + \frac{V_1}{(2\overline{x})^{1/2}} + V_2 + \frac{\mathrm{e}^{\mathrm{i}\overline{x}}}{\kappa_2 (2\overline{x})^{1/2}} + \mathrm{e}^{\mathrm{i}\overline{x}} \left(-\frac{\beta}{4\overline{x}} + \frac{g_1^{(0)}}{(2\overline{x})^{1/2}} + g_2^{(0)} \right) \\ & + \mathrm{e}^{\mathrm{i}\overline{x} + \mathrm{i}\kappa_2 (2\overline{x})^{1/2}\overline{\eta} - \kappa_2^2 \overline{x}} \left(\frac{\beta}{2\overline{x}} - \frac{1 + \mathrm{i}\kappa_2^2}{\kappa_2 (2\overline{x})^{1/2}} \right) - \frac{\beta}{4\overline{x}} - \frac{g_1^{(0)} - \mathrm{i}\kappa_2 (1 - \beta\overline{\eta})}{(2\overline{x})^{1/2}} \\ & - g_2^{(0)} + \beta\kappa_2^2/2 - \mathrm{i}\beta/4 + \overline{\eta} \left(i - \kappa_2^2 \right) + \beta\kappa_2^2 \overline{\eta}^2/2, \end{aligned} \quad \text{(B6)}$$

$$\begin{aligned} \frac{\partial \overline{p}^{(0)}}{\partial \eta} \to {} & \frac{P_0'}{(2\overline{x})^{3/2}} + \frac{P_1'}{2\overline{x}} + \frac{P_2'}{(2\overline{x})^{1/2}} - \frac{\beta \mathrm{e}^{\mathrm{i}\overline{x}}}{4\overline{x}} - g_2^{(0)} \mathrm{e}^{\mathrm{i}\overline{x}} - \mathrm{i}\beta \mathrm{e}^{\mathrm{i}\overline{x}}/4 \\ & + \beta \overline{x}^{-1} \mathrm{e}^{\mathrm{i}\overline{x} + \mathrm{i}\kappa_2 (2\overline{x})^{1/2}\overline{\eta} - \kappa_2^2 \overline{x}} - \frac{3\beta}{4\overline{x}} - \frac{2\mathrm{i}\beta\overline{\eta}\kappa_2}{(2\overline{x})^{1/2}}. \end{aligned}$$

The outer boundary conditions for the power series equations become

$$U_1 \to \mathrm{i}\kappa_2 \overline{\eta}, \ U_2 \to \left(\mathrm{i} - \kappa_2^2 (1 + \overline{\eta}^2)\right)/2 \text{ as } \eta \to \infty,$$

and the constants simplify to

$$g_1^{(0)} = V_{1,0} + \mathrm{i}\kappa_2 (1 + \beta^2), \ g_2^{(0)} = V_{2,0} - 5\mathrm{i}\beta/4 + 3\beta\kappa_2^2/2 + \beta^3 \kappa_2^2/2,$$
$$V_{2,1} = \kappa_2^2 - \mathrm{i}, \ V_{2,2} = -\beta\kappa_2^2/2.$$

Figure 16 displays the profiles of the amplitude of the streamwise $\overline{u}^{(0)}$ and wall-normal $\overline{v}^{(0)}$ velocity components for $\kappa = 0$, $\kappa_2 = 1$ at $\overline{x} = 7 \times 10^{-4}$ obtained by the initial conditions (B1) and (B2) (or (B5) and (B6) in this two-dimensional case). The inner solutions are given by the power series terms in (2.30). The outer solutions are

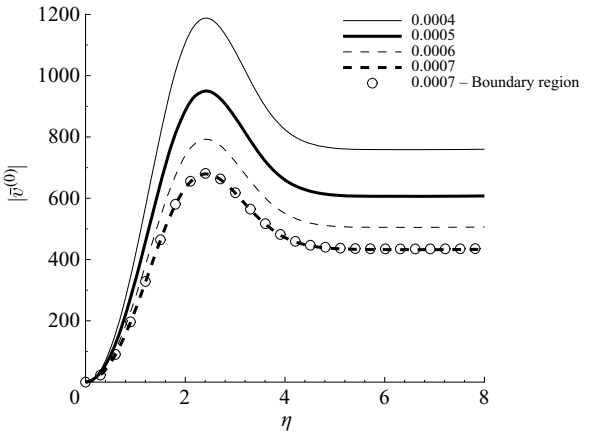

FIGURE 17. Amplitude of wall-normal $\bar{v}^{(0)}$ velocity profiles for $\kappa = 0$ and $\kappa_2 = 1$ at different streamwise locations $\bar{x} \ll 1$ obtained by (B2) (solid lines) and by solving numerically the LUBR equations (2.9)–(2.12) with one downstream step ($\Delta\bar{x} = 10^{-4}$) (circles).

the terms including the exponentials in (B1) and (B2). The common parts are given by the remaining terms in (B1) and (B2).

Figure 17 shows the profiles of the amplitude of $\bar{v}^{(0)}$ for $\kappa = 0$, $\kappa_2 = 1$ at different streamwise locations $\bar{x} \ll 1$ obtained by the composite solution (B2). The profile at $\bar{x} = 7 \times 10^{-4}$ is successfully compared with the solution computed by integrating the LUBR equation by one step ($\Delta\bar{x} = 10^{-4}$).

REFERENCES

ALLEN, L. & BRIDGES, T. B. 2003*a* Hydrodynamic stability of the Ekman boundary layer including interaction with a compliant surface: a numerical framework. *Eur. J. Mech.* B **22**, 239–258.

ALLEN, L. & BRIDGES, T. J. 2002 Numerical exterior algebra and the compound matrix method. *Numer. Math.* **92**, 197–232.

ALLEN, L. & BRIDGES, T. J. 2003*b* Flow past a swept wing with a compliant surface: stabilizing the attachment-line boundary layer. *Studies Appl. Math.* **110**, 333–349.

ANDERSSON, P., BERGGREN, M. & HENNINGSON, D. S. 1999 Optimal disturbances and bypass transition in boundary layers. *Phys. Fluids* **11** (1), 134–150.

ANTHONY, R. J., JONES, T. V. & LAGRAFF, J. E. 2005 High frequency surface heat flux imaging of bypass transition. *J. Turbom.* **127**, 241–250.

ARNAL, D. & JUILLEN, J. C. 1978 Contribution expérimental a l'etude de la receptivite d'une couche limite laminaire, a la turbulence de l'ecoulement general. *Rep. No.* CERT RT 1/5018 AYD. ONERA.

BATCHELOR, G. K. 1946 The theory of axisymmetric turbulence. *Proc. R. Soc. Lond.* A **186** (1007), 480–502.

BRADSHAW, P. 1965 The effect of wind-tunnel screens on nominally two-dimensional boundary layers. *J. Fluid Mech.* **22**, 679–687.

CEBECI, T. 2002 *Convective Heat Transfer*. Springer.

CHANDRASEKHAR, S. 1950 The theory of axisymmetric turbulence. *Proc. R. Soc. Lond.* A **242** (855), 557–577.

CHOUDHARI, M. 1994*a* Localized and distributed boundary-layer receptivity to convected unsteady wake in free stream. *Contractor Rep.* 4578. NASA Langley Research Center.

CHOUDHARI, M. 1994*b* Roughness-induced generation of crossflow vortices in three-dimensional boundary layers. *Theoret. Comput. Fluid Dyn.* **6**, 1–30.

CHOUDHARI, M. 1996 Boundary layer receptivity to three-dimensional unsteady vortical disturbances in the free stream. *Paper* 96-0181. AIAA.

Choudhari, M. & Streett, C. L. 1992 A finite Reynolds number approach for the prediction of boundary-layer receptivity in localized regions. *Phys. Fluids* **4** (11), 2495–2514.

Crow, S. C. 1966 The spanwise perturbation of two-dimensional boundary-layers. *J. Fluid Mech.* **24**, 153–164.

Davey, A. 1982 A difficult numerical calculation concerning the stability of the Blasius boundary layer. In *Stability in the Mechanics of Continua* (ed. F. H. Schroeder), pp. 365–372. Springer.

Dietz, A. J. 1996 Distributed boundary layer receptivity to convected vorticity. *Paper* 96-2083. AIAA.

Dietz, A. J. 1998 Boundary-layer receptivity to transient convected disturbances. *AIAA J.* **36**, 1171–1177.

Dietz, A. J. 1999 Local boundary-layer receptivity to a convected free-stream disturbance. *J. Fluid Mech.* **378**, 291–317.

Dryden, H. L. 1936 Air flow in the boundary layer near a plate. *Rep.* 562. NACA.

Duck, P. W., Ruban, A. I. & Zhikharev, C. N. 1996 The generation of Tollmien--Schlichting waves by free-stream turbulence. *J. Fluid Mech.* **312**, 341–371.

Ellingsen, T. & Palm, E. 1975 Stability of linear flow. *Phys. Fluids* **18** (4), 487–488.

Fasel, H. 2002 Numerical investigation of the interaction of the Klebanoff-mode with a Tollmien–Schlichting wave. *J. Fluid Mech.* **450**, 1–33.

Fransson, J. H. M., Matsubara, M. & Alfredsson, P. H. 2005 Transition induced by free-stream turbulence. *J. Fluid Mech.* **527**, 1–25.

Goldstein, M. E. 1978 Unsteady vortical and entropic distortions of potential flows round arbitrary obstacles. *J. Fluid Mech.* **89**, 433–468.

Goldstein, M. E. 1983 The evolution of Tollmein–Schlichting waves near a leading edge. *J. Fluid Mech.* **127**, 59–81.

Goldstein, M. E. 1985 Scattering of acoustic waves into Tollmien–Schlichting waves by small streamwise variations in surface geometry. *J. Fluid Mech.* **154**, 509–529.

Goldstein, M. E. & Leib, S. J. 1993 Three-dimensional boundary layer instability and separation induced by small-amplitude streamwise vorticity in the upstream flow. *J. Fluid Mech.* **246**, 21–41.

Goldstein, M. E., Leib, S. J. & Cowley, S. J. 1992 Distortion of a flat plate boundary layer by free stream vorticity normal to the plate. *J. Fluid Mech.* **237**, 231–260.

Goldstein, M. E. & Sescu, A. 2008 Boundary-layer transition at high free-stream disturbance levels – beyond Klebanoff modes. *J. Fluid Mech.* **613**, 95–124.

Goldstein, M. E. & Wundrow, D. W. 1998 On the environmental realizability of algebraically growing disturbances and their relation to Klebanoff modes. *Theoret. Comput. Fluid Dyn.* **10**, 171–186.

Gulyaev, A. N., Kozlov, V. E., Kuzenetsov, V. R., Mineev, B. I. & Sekundov, A. N. 1989 Interaction of a laminar boundary layer with external turbulence. *Izv. Akad. Nauk. SSSR Mekh. Zhid. Gaza* **6**, 700–710.

Hernon, D., Walsh, E. J. & McEligot, D. M. 2007 Experimental investigation into the routes to bypass transition and the shear-sheltering phenomenon. *J. Fluid Mech.* **591**, 461–479.

Huang, J-C. & Johnson, M. W. 2007 The influence of compliant surfaces on bypass transition. *Exp. Fluids* **42**, 711–718.

Inasawa, A., Lundell, F., Matsubara, M., Kohama, Y. & Alfredsson, P. H. 2003 Velocity statistics and flow structures observed in bypass transition using stereo PTV. *Exp. Fluids* **34**, 242–252.

Jacobs, R. G. & Durbin, P. A. 2001 Simulation of bypass transition. *J. Fluid Mech.* **428**, 185–212.

Kemp, N. 1951 The laminar three-dimensional boundary layer and a study of the flow past a side edge. MSc thesis, Cornell University, Ithaca, NY.

Kendall, J. M. 1985 Experimental study of disturbances produced in a pre-transitional boundary layer. *Paper 85-1695*. AIAA.

Kendall, J. M. 1990 Boundary layer receptivity to free stream turbulence. *Paper* 90-1504. AIAA.

Kendall, J. M. 1991 Studies on laminar boundary layer receptivity to free-stream turbulence near a leading edge. In *Boundary Layer Stability and Transition to Turbulence* (ed. D. C. Reda, H. L. Reed & R. Kobayashi), vol. 114, pp. 23–30. ASME FED.

Kerschen, E. J. 1991 Linear and nonlinear receptivity to vortical free-stream disturbances. In *Boundary Layer Stability and Turbulence* (ed. D. C. Reda, H. L. Reed & R. K. Kobayashi), vol. 114, pp. 43–48. ASME FED.

Kim, J., Moin, P. & Moser, R. 1987 Turbulence statistics in fully developed channel flow at low Reynolds number. *J. Fluid Mech.* **177**, 133–166.

Klebanoff, P. S. 1971 Effect of free-stream turbulence on a laminar boundary layer. *Bull. Am. Phys. Soc.* **16**, 1323.

Landahl, M.T. 1980 A note on an algebraic instability of inviscid parallel shear flows. *J. Fluid Mech.* **98**, 243–251.

Lardeau, S., Li, N. & Leschziner, M. A. 2007 Large eddy simulations of a transitional boundary layers at high free-stream turbulence intensity and implications for RANS modelling. *J. Turbom.* **129**, 1–7.

Leib, S. J., Wundrow, D. W. & Goldstein, M. E. 1999 Effect of free-stream turbulence and other vortical disturbances on a laminar boundary layer. *J. Fluid Mech.* **380**, 169–203.

Liu, Y., Zaki, T. A. & Durbin, P. A. 2008 Boundary-layer transition by interaction of discrete and continuous modes. *J. Fluid Mech.* **604**, 199–233.

Luchini, P. 2000 Reynolds-number-independent instability of the boundary layer over a flat surface: optimal perturbations. *J. Fluid Mech.* **404**, 289–309.

Malik, M. R. 1990 Numerical methods for hypersonic boundary layer stability. *J. Comput. Phys.* **86**, 376–413.

Mans, J., Kadijk, E. C., de Lange, H. C. & van Steenhoven, A. A. 2005 Breakdown in a boundary layer exposed to free-stream turbulence. *Exp. Fluids* **39**, 1071–1083.

Matsubara, M. & Alfredsson, P. H. 2001 Disturbance growth in boundary layers subjected to free-stream turbulence. *J. Fluid Mech.* **430**, 149–168.

Nagarajan, S., Lele, S. K. & Ferziger, J. H. 2007 Leading-edge effects in bypass transition. *J. Fluid Mech.* **572**, 471–504.

Ng, B. S. & Reid, W. H. 1979 An initial value method for eigenvalue problems using compound matrices. *J. Comput. Phys.* **30**, 125–136.

Orr, W. M. F. 1907 The stability or instability of steady motions of a perfect liquid and of a viscous liquid. Part I. A perfect liquid. Part II. A viscous liquid. *Proc. R. Irish Acad.* **27**, 9–38 and 69–138.

Ovchinnikov, V., Choudhari, M. M. & Piomelli, U. 2008 Numerical simulations of boundary-layer bypass transition due to high-amplitude free-stream turbulence. *J. Fluid Mech.* **613**, 135–169.

Ricco, P., Tran, D.-L. & Ye, G. 2009 Wall heat transfer effects on Klebanoff modes and Tollmien–Schlichting waves in a compressible boundary layer. *Phys. Fluids* **21**, 1–18 (024106).

Ricco, P. & Wu, X. 2007 Response of a compressible laminar boundary layer to free-stream vortical disturbances. *J. Fluid Mech.* **587**, 97–138.

Ruban, A. I. 1985 On the generation of Tollmien–Schlichting waves by sound. *Fluid Dyn.* **25** (2), 213–221.

Schewe, G. 1983 On the structure and resolution of wall-pressure fluctuations associated with turbulent boundary-layer flow. *J. Fluid Mech.* **134**, 311–328.

Schlichting, H. 1933 Zur Entstehung der Turbulenz bei der Plattenströmung. *Nachr. Ges. Wiss. Göttingen Math. Phys. Klasse*, 181–208.

Schubauer, G. B. & Skramstad, H. K 1947 Laminar boundary-layer oscillations and transition on a flat plate. *Rep. No.* NACA-TN-909. NACA.

Sengupta, T. K. 1992 Solution of the Orr–Sommerfeld equation for high wavenumbers. *Comput. Fluids* **21** (2), 301–303.

Sengupta, T. K. & Subbaiah, K. V. 2006 Spatial stability for mixed convection boundary layer over a heated horizontal plate. *Studies Appl. Math.* **117**, 265–298.

Sobey, I. J. 2001 *Introduction to Interactive Boundary Layer Theory*. Oxford University Press.

Sommerfeld, A. 1908 Ein Beitrag zur hydrodynamischen Erklarung der turbulenten Flussigkeitsbewegungen. *Atti Fourth Congr. Intl Math. Roma* **3**, 116–124.

Spalart, P. R. 1988 Direct simulation of a turbulent boundary layer up to $Re_\theta = 1410$. *J. Fluid Mech.* **187**, 61–98.

Taylor, G. I. 1939 Some recent developments in the study of turbulence. In *Fifth International Congress for Applied Mechanics* (ed. J. P. Den Hartog & H. Peters), pp. 294–310. Wiley/Chapman and Hall.

Tollmien, W. 1929 Uber die Entstehung der Turbulenz 1. Mitteilung. *Nachr. Ges. Wiss. Göttingen Math. Phys. Klasse*, 21–44. Translated into English in 1931 as as *Rep. No.* NACA-TM-609, NACA.

Tsuji, Y., Fransson, J. H. M., Alfredsson, P. H. & Johansson, A. V. 2007 Pressure statistics and their scaling in high-Reynolds-number turbulent boundary layers. *J. Fluid Mech.* **585**, 1–40.

Volino, R. 2005 An investigation of the scales in transitional boundary layers under high free-stream turbulence conditions. *Exp. Fluids* **38**, 516–533.

Watmuff, J. H. 1998 Detrimental effects of almost immensurably small free stream nonuniformities generated by wind-tunnel screens. *AIAA J.* **36** (3), 379–386.

Westin, K. J. A., Boiko, A. V., Klingmann, B. G. B., Kozlov, V. V. & Alfredsson, P. H. 1994 Experiments in a boundary layer subjected to free stream turbulence. Part 1. Boundary layer structure and receptivity. *J. Fluid Mech.* **281**, 193–218.

Wiegel, M. & Wlezien, R. W. 1993 Acoustic receptivity of laminar boundary layers over wavy walls. *Paper* 93-3280. AIAA.

Wu, X. 2001*a* On local boundary-layer receptivity to vortical disturbances in the free-stream. *J. Fluid Mech.* **449**, 373–393.

Wu, X. 2001*b* Receptivity of boundary layers with distributed roughness to vortical and acoustic disturbances: A second-order asymptotic theory and comparison with experiments. *J. Fluid Mech.* **431**, 91–133.

Wu, X. & Choudhari, M. 2003 Linear and nonlinear instabilities of a Blasius boundary layer perturbed by streamwise vortices. Part 2. Intermittent instability induced by long-wavelength Klebanoff modes. *J. Fluid Mech.* **483**, 249–286.

Wundrow, D. W. & Goldstein, M. E. 2001 Effect on a laminar boundary layer of small-amplitude streamwise vorticity in the upstream flow. *J. Fluid Mech.* **426**, 229–262.